IPMU21–0074, KEK–TH–2366, OU–HET–1115, P3H–21–090, TTP21–046

Non-resonant new physics search at the LHC for the $b \to c\tau\nu$ anomalies

Motoi Endo,[a,b,c] **Syuhei Iguro,**[c,d,e,f] **Teppei Kitahara,**[g,h] **Michihisa Takeuchi,**[h,i] **and Ryoutaro Watanabe**[j]

[a] *KEK Theory Center, IPNS, KEK, Tsukuba 305–0801, Japan*
[b] *The Graduate University of Advanced Studies (Sokendai), Tsukuba 305–0801, Japan*
[c] *Kavli Institute for the Physics and Mathematics of the Universe (WPI), The University of Tokyo Institutes for Advanced Study, The University of Tokyo, Kashiwa 277–8583, Japan*
[d] *Department of Physics, Nagoya University, Nagoya 464–8602, Japan*
[e] *Institute for Theoretical Particle Physics (TTP), Karlsruhe Institute of Technology (KIT), Engesserstraße 7, 76131 Karlsruhe, Germany*
[f] *Institute for Astroparticle Physics (IAP), Karlsruhe Institute of Technology (KIT), Hermann-von-Helmholtz-Platz 1, 76344 Eggenstein-Leopoldshafen, Germany*
[g] *Institute for Advanced Research, Nagoya University, Nagoya 464–8601, Japan*
[h] *Kobayashi-Maskawa Institute for the Origin of Particles and the Universe, Nagoya University, Nagoya 464–8602, Japan*
[i] *Department of Physics, Osaka University, Toyonaka 560–0043, Japan*
[j] *INFN, Sezione di Pisa, Largo Bruno Pontecorvo 3, I-56127 Pisa, Italy*

E-mail: motoi.endo@kek.jp, igurosyuhei@gmail.com, teppeik@kmi.nagoya-u.ac.jp, m.takeuchi@het.phys.sci.osaka-u.ac.jp, wryou1985@gmail.com

ABSTRACT: Motivated by the $b \to c\tau\overline{\nu}$ anomalies, we study non-resonant searches for new physics at the large hadron collider (LHC) by considering final states with an energetic and hadronically decaying τ lepton, a b-jet and large missing transverse momentum ($pp \to \tau_h \bar{b} + E_{\rm T}^{\rm miss}$). Such searches can be useful to probe new physics contributions to $b \to c\tau\overline{\nu}$. They are analyzed not only within the dimension-six effective field theory (EFT) but also in explicit leptoquark (LQ) models with the LQ non-decoupled. The former is realized by taking a limit of large LQ mass in the latter. It is clarified that the LHC sensitivity is sensitive to the LQ mass for $\mathcal{O}(1)$ TeV even in the search of $pp \to \tau_h \bar{b} + E_{\rm T}^{\rm miss}$. Although the LQ models provide a weaker sensitivity than the EFT limit, it is found that the non-resonant search of $pp \to \tau_h \bar{b} + E_{\rm T}^{\rm miss}$ can improve the sensitivity by $\approx 40\%$ versus a conventional mono-τ search ($pp \to \tau_h + E_{\rm T}^{\rm miss}$) in the whole LQ mass region. Consequently, it is expected that most of the parameter regions suggested by the $b \to c\tau\overline{\nu}$ anomalies can be probed at the HL-LHC. Also, it is shown that R_2 LQ scenario is accessible entirely once the LHC Run 2 data are analyzed. In addition, we discuss a charge selection of τ_h to further suppress the standard-model background, and investigate the angular correlations among b, τ and the missing transverse momentum to discriminate the LQ scenarios.

KEYWORDS: Flavor physics, LHC, Beyond Standard Model, Effective Field Theories, Leptoquark

Contents

1 Introduction

Semi-leptonic B-meson decay processes have been investigated to test the Standard Model (SM) and to search for a hint for New Physics (NP). In the last decade, the BaBar [1, 2], Belle [3–7] and LHCb collaborations [8–10] have reported exiting anomalies in semi-leptonic decays of B mesons, such as $R_{D^{(*)}} = \mathrm{BR}(B \to D^{(*)}\tau\overline{\nu})/\mathrm{BR}(B \to D^{(*)}\ell\overline{\nu})$, with $\ell = \mu$ for LHCb and an average of e and μ for BaBar and Belle. Here, a ratio of the branching ratios is taken to reduce both experimental and theoretical (*i.e.*, parametric and QCD) uncertainties significantly, so that $R_{D^{(*)}}$ is sensitive to NP that couples to quarks and leptons. Although the latest result released by Belle becomes closer to the SM values [6, 7], the world average of $R_{D^{(*)}}$ measurements still deviates from the SM predictions at the 3–4 σ confidence level (CL) (see Ref. [11] for a recent summary of the SM predictions).

The $R_{D^{(*)}}$ discrepancy suggests violation of the lepton flavor universality (LFU) between τ and light leptons, and has prompted many attempts of the NP introducing new scalar and vector mediators (see, *e.g.*, Ref. [12] for the very recent review). In terms of the low-energy effective Hamiltonian, their contributions are encoded as

$$\begin{aligned}\mathcal{H}_{\rm eff} = 2\sqrt{2}G_F V_{cb}\Big[&(1+C_{V_1})(\bar{c}\gamma^\mu P_L b)(\bar{\tau}\gamma_\mu P_L \nu_\tau) + C_{V_2}(\bar{c}\gamma^\mu P_R b)(\bar{\tau}\gamma_\mu P_L \nu_\tau)\\ &+ C_{S_1}(\bar{c}P_R b)(\bar{\tau}P_L \nu_\tau) + C_{S_2}(\bar{c}P_L b)(\bar{\tau}P_L \nu_\tau)\\ &+ C_T(\bar{c}\sigma^{\mu\nu}P_L b)(\bar{\tau}\sigma_{\mu\nu}P_L \nu_\tau)\Big] + \text{h.c.}\,, \end{aligned} \tag{1}$$

with $P_{L/R} = (1 \mp \gamma_5)/2$.[#1][#2] Here, the Wilson coefficients (WCs), C_X, are normalized by the SM contribution, $\mathcal{H}_{\rm eff} = 2\sqrt{2}G_F V_{cb}(\bar{c}\gamma^\mu P_L b)(\bar{\tau}\gamma_\mu P_L \nu_\tau)$, corresponding to $C_X = 0$ for $X = V_{1,2}, S_{1,2}, T$. Note that the SM contribution is suppressed by the Cabibbo-Kobayashi-Maskawa (CKM) matrix element V_{cb} [19, 20], where $V_{cb} = 0.041$ [21] is set throughout this paper. One can see that a scale of NP implied by the $R_{D^{(*)}}$ anomaly is restricted as $\lesssim \mathcal{O}(10)$ TeV by the perturbative unitarity limit on NP interactions [22].

The large hadron collider (LHC) experiment has a great potential to test such NP contributions. They can be probed, *e.g.*, by resonant searches for new particles such as charged Higgs, W' (and related Z'), and leptoquark (LQ), and by non-resonant searches for the contact interactions of Eq. (1). In addition to various flavor measurements, *e.g.*, $B_c \to \tau\bar{\nu}$, $\Lambda_b \to \Lambda_c \tau\bar{\nu}$, and polarization observables in $B \to D^{(*)}\tau\bar{\nu}$ in the near future, which have been studied to check those contributions, the collider searches provide independent information. Moreover, they are free from uncertainties of the flavor observables especially inherent in $B \to D^{(*)}$ hadronic form factors.

In this paper, we examine non-resonant searches in light of the $R_{D^{(*)}}$ anomaly. Even if new particles are heavier than the LHC beam collision energy, their contributions could be detected indirectly by exchanging these particles in t-channel propagators. The ATLAS and CMS collaborations have performed non-resonant searches especially to probe W' boson (with assuming a decay $W' \to \tau\nu$) in the sequential standard model. They have done a $\tau\nu$ search, *i.e.*, analyzed events with a hadronic τ jet and a large missing transverse momentum by using the Run 1 and 2 data [23–26]. The results are consistent with the SM background (BG) expectations, and one can use them to set upper bounds on the NP interactions relevant to the $R_{D^{(*)}}$ anomaly, or the operators in Eq. (1). References [27–30] have studied such an interplay, *i.e.*, the relation between the high-$p_{\rm T}$ tail of the $\tau\nu$ events at the LHC and the $R_{D^{(*)}}$ anomaly in new physics models.

Recently, it has been pointed out that sensitivities to the NP may be improved versus the above non-resonant $\tau\nu$ search by requiring an additional b-jet in the final state [31–33]. This can be understood from the fact that the genuine $\tau\nu + b$ final state is achieved by $gq \to b\tau\nu$ ($q = u, c$) within the SM. Since this contribution is suppressed by $|V_{ub\,(cb)}|^2 \sim \mathcal{O}(10^{-5\,(-3)})$, the main SM background comes from $\tau\nu + j$ events with mis-identifying a light-flavored jet as b jet. This is in contrast to the $\tau\nu$ search, whose SM contributions, *e.g.*, $\bar{u}d \to \tau\bar{\nu}$, are not suppressed by the CKM factors or mis-identifications. In addition, the additional b quark allows us to study

[#1] The Wilson coefficients are also shown as $C_{V_1} = C_V^L$, $C_{V_2} = C_V^R$, $C_{S_1} = C_S^R$, and $C_{S_2} = C_S^L$ [13].

[#2] In this paper, right-handed neutrinos are not considered (or equivalently assumed to be heavier than the B meson). See Refs. [14–18] for models with light right-handed neutrinos in the context of the $R_{D^{(*)}}$ anomaly.

angular correlations among the final state particles, which are potentially useful to distinguish the NP interactions. Such a channel has been studied in Ref. [34] for general NP contact interactions, including those relevant to the $R_{D^{(*)}}$ anomaly. They have argued that sensitivities to each WC searches can be improved by $\sim 30\%$ versus the $\tau\nu$ search. Moreover, it was argued that angular correlations between b and τ or ν would be useful to distinguish possible NP scenarios working in the center of mass frame.

After the above analyses, there are significant developments within the context of the $\tau\nu$ search. In the previous studies, the effective field theory (EFT) approach (*i.e.*, the contact-interaction approximation) had been taken to describe the NP contributions. However, as pointed out in Ref. [35], this prescription is not always appropriate to represent actual NP contributions when the LHC non-resonant search is studied. In fact, a transverse mass defined as

$$m_{\rm T} = \sqrt{2p_{\rm T}^{\tau}E_{\rm T}^{\rm miss}\left[1-\cos\Delta\phi(\vec{p}_{\rm T}^{\,\tau},\vec{p}_{\rm T}^{\,\rm miss})\right]}\,, \tag{2}$$

is often introduced to analyze high-$p_{\rm T}$ events, where $\Delta\phi$ is a relative angle ($0 \le \Delta\phi \le \pi$) and the missing transverse momentum is expressed by $\vec{p}_{\rm T}^{\,\rm miss}$ with magnitude $E_{\rm T}^{\rm miss}$. Since a new particle appearing in the t-channel propagator is likely to carry a large momentum transfer to produce a high-$p_{\rm T}$ τ lepton and it produces an effective new particle mass (since $t < 0$),

$$\mathcal{M}_{\rm LQ} \approx \frac{g_{\rm LQ}^2}{\left|t - M_{\rm LQ}^2\right|} < \frac{g_{\rm LQ}^2}{M_{\rm LQ}^2} \approx \mathcal{M}_{\rm EFT}\,, \tag{3}$$

the EFT description is no longer appropriate. We can see that sensitivities to the NP tend to become weaker than those in the EFT description, which is valid only for $M_{\rm LQ} \gg m_{\rm T}$. Although the study in Ref. [35] has been done for the non-resonant $\tau\nu$ search, a similar conclusion can hold for the $\tau\nu + b$ case. In this paper, it will be shown that the sensitivity to the WCs can be weakened by up to 50% even for $\tau\nu + b$.

Moreover, it is pointed out that the NP sensitivity can be improved by choosing negative-charge mono-τ events [35]. This follows from the fact that the dominant SM background comes from $pp \to W^{\pm(*)} \to \tau^{\pm}\nu$, and then the imbalance of $N(W^+)/N(W^-) > 2$ is observed due to reflecting the proton charge [36, 37]. This is in contrast to the NP case: the interaction in Eq. (1) predicts $N(\tau^+)/N(\tau^-) = 1$ because the contribution is not generated from valence quarks. In fact, in order to distinguish the charge of the τ jet, one has to observe a sagitta of the charged pion from the τ decay. In the high-$p_{\rm T}$ region such as $p_{\rm T}^{\pi^{\pm}} = 1$ TeV, the sagitta in the CMS inner detector becomes $\mathcal{O}(100)\,\mu$m. Since this is larger than the detector resolution, the charge of τ jet with $p_{\rm T}^{\tau} = \mathcal{O}(1)$ TeV could be distinguished with good accuracy. Therefore, it is important to study impacts of the charge selection.

In this paper, we perform a comprehensive analysis of the non-resonant $\tau\nu + b$ search as well as the $\tau\nu$ one with adopting the above developments. We also discuss directions of further improvements of the NP sensitivity especially to distinguish the NP interaction operators, *e.g.*, by utilizing the charge asymmetry of $\tau^{\pm}$ and the angular correlations among the final states.

This paper is organized as follows. A model setup is explained in Sec. 2. A strategy to generate the background and signal events is explained in Sec. 3. Numerical results and future prospects are explored in Sec. 4. Impacts of their sensitivities on the NP interpretation for the notorious $R_{D^{(*)}}$ anomaly are also given in this section. Section 5 is devoted to conclusions and discussion.

2 New physics scenarios

In this paper, leptoquark (LQ) models are employed as an illustrative realization of the WCs of the effective Hamiltonian in Eq. (1). They form the WCs at the NP scale $\Lambda \sim M_{\rm LQ}$ as

$$2\sqrt{2}G_F V_{cb} C_X(\Lambda) = N_X \frac{h_1 h_2}{M_{\rm LQ}^2}, \tag{4}$$

with LQ mass $M_{\rm LQ}$ and LQ couplings to the SM fermions $h_{1,2}$. The numerical factor N_X depends on the Lorenz structure of the EFT operator ($X = V_{1,2}, S_{1,2}, T$).

We are interested in NP scenarios that can explain the $R_{D^{(*)}}$ anomaly. Solutions to the anomaly are given in terms of C_X in the literature, *e.g.*, see Refs. [35, 38, 39]. A general consensus is, for instance, that scenarios with a single NP operator $X = V_{1,2}$ work well, which can be realized in particular LQ models. Also, there are LQ models which contribute to multiple WCs.

Given the LQ mass $M_{\rm LQ}$, the high-$p_{\rm T}$ search puts an upper bound on the LQ couplings and the WCs in Eq. (1) at the $\Lambda_{\rm LHC}$ scale, which is encoded as $C_X(\Lambda_{\rm LHC})$ in this paper. The LHC scale reflects the high-$p_{\rm T}$ region sensitive to the NP signal. Hence, in the following analysis, we take a typical size as $\Lambda_{\rm LHC} = 1$ TeV, which is the same as Ref. [34]. In the flavor physics, the EFT limit $q^2 \ll \Lambda^2$ is a good approximation for $\Lambda \gtrsim \mathcal{O}(100)$ GeV. However, as mentioned in the introduction, this is not the case for the high-$p_{\rm T}$ searches at the LHC, where $p_{\rm T}$ can be $\mathcal{O}(1)$ TeV. Thus, we will investigate explicit $M_{\rm LQ}$ dependences of the sensitivities of $C_X(\Lambda_{\rm LHC})$.

In the following subsections, we show explicit LQ models to setup the NP scenarios of our interest and also give a brief explanation for collider signatures.

2.1 U_1 LQ

The $SU(2)_L$ singlet vector LQ (U_1) is one of the well-known candidates to explain several B anomalies [40, 41]. Its interaction is written as

$$\mathcal{L}_{\mathrm{U}_1\mathrm{LQ}} = h_L^{ij}\left(\bar{u}_i \gamma_\mu P_L \nu_j + \bar{d}_i \gamma_\mu P_L \ell_j\right)\mathrm{U}_1^\mu + h_R^{ij}\left(\bar{d}_i \gamma_\mu P_R \ell_j\right)\mathrm{U}_1^\mu + \mathrm{h.c.}. \tag{5}$$

By integrating out the LQ, one can obtain two WCs as

$$2\sqrt{2}G_F V_{cb} C_{V_1} = +\frac{(V_{\rm CKM} h_L)^{23} h_L^{*33}}{M_{\rm LQ}^2}, \qquad 2\sqrt{2}G_F V_{cb} C_{S_1} = -2\frac{(V_{\rm CKM} h_L)^{23} h_R^{*33}}{M_{\rm LQ}^2}. \tag{6}$$

It is noticed that these WCs depend on different couplings, *i.e.*, are independent with each other. The couplings irrelevant to $b \to c\tau\overline{\nu}$ are assumed to be zero.

The scenario with $C_{V_1} \neq 0$ and $C_{S_1} = 0$, so-called the single C_{V_1} scenario, is realized by taking $h_R^{*33} = 0$, which will be investigated later. Note that $C_{V_1} \neq 0$ can also be obtained by other LQ models such as the $SU(2)_L$ triplet vector (U_3), singlet scalar (S_1), and triplet scalar (S_3) LQs. However, these models confront a stringent constraint from $b \to s\nu\overline{\nu}$ unavoidably in single LQ scenarios at the tree level, see Appendix B. For instance, $|C_{V_1}| \lesssim 0.03$ is obtained for the S_1 LQ scenario, which is not consistent with the $R_{D^{(*)}}$ solution, $C_{V_1} = 0.09 \pm 0.02$. Hence, the U_1 LQ is the only possibility to realize this scenario (see Ref. [42] for alternative possibility by use of multiple LQs). Note that the constraints from ΔM_s and $\Delta M_s/\Delta M_d$ are UV-model dependent. For

U_1 LQ models, additional vector-like leptons are often incorporated in the UV models. These constraints are weakened by incorporating light vector-like leptons contributions via a GIM-like mechanism [43, 44].

Another scenario has been discussed in the context of a $U(2)$ flavor symmetry [45–52]. In this scenario, h_L and h_R are aligned, and the two WCs are related as

$$C_{S_1} = -2\beta_R C_{V_1}\,, \tag{7}$$

where $\beta_R = e^{i\phi_R}$ denotes a relative phase [52]. Assuming C_{V_1} to be real, the result to explain the $R_{D^{(*)}}$ anomaly is given as $\phi_R \sim 0.4\pi$ and $C_{V_1} \sim 0.09$. This scenario will also be investigated in this paper. Note that the LHC study is less sensitive to the phase.

2.2 R_2 LQ

The $SU(2)_L$ doublet scalar LQ (R_2) also provides distinctive solutions to the $R_{D^{(*)}}$ anomaly. A *practical* R_2 LQ model introduces two distinct LQ doublets, $\mathbf{R}_{2,1} = (\mathrm{R}_{2,1}^{5/3}, \mathrm{R}_{2,1}^{2/3})$ and $\mathbf{R}_{2,2} = (\mathrm{R}_{2,2}^{2/3}, \mathrm{R}_{2,2}^{-1/3})$, in the SM gauge invariant form, for which a large mixing between $\mathrm{R}_{2,1}^{2/3}$ and $\mathrm{R}_{2,2}^{2/3}$ is induced via an electroweak symmetry breaking term; $\mathrm{R}_{2,1}^{2/3}\mathrm{R}_{2,2}^{-2/3}(H^{0*})^2$. Then, the interaction of the mass eigenstate $\mathrm{R}_2^{2/3}$ is picked out as

$$\mathcal{L}_{\mathrm{R_2LQ}} = \left(h_L^{ij}\overline{u}_i P_L \nu_j + h_R^{ij}\overline{d}_i P_R \ell_j + \tilde{h}_L^{ij}\overline{d}_i P_L \ell_j\right)\mathrm{R}_2^{2/3} + \mathrm{h.c.}\,. \tag{8}$$

Then three WCs are generated, two of which are related, as

$$2\sqrt{2}G_F V_{cb} C_{V_2} = +\frac{h_L^{23}\tilde{h}_L^{*33}}{2M_{\mathrm{LQ}}^2}\,, \qquad 2\sqrt{2}G_F V_{cb} C_{S_2} = +\frac{h_L^{23}h_R^{*33}}{2M_{\mathrm{LQ}}^2}\,, \qquad C_{S_2} = +4C_T\,. \tag{9}$$

Both two scenarios, namely the one with the single C_{V_2} and another for the specific combination $C_{S_2} = +4C_T$, can solve the $R_{D^{(*)}}$ anomaly. Hence, collider studies will be performed for them in this paper.

Here, the coupling $\tilde{h}_L$ is generated from the mixing above the electroweak symmetry breaking scale. This implies that C_{V_2} should have an additional suppression factor. See Ref. [53] for a UV completion of the C_{V_2} scenario and its phenomenological bounds. It will be shown that there are still viable parameter regions. Nevertheless, our collider study provides a useful probe for the C_{V_2} constraint as we will see in Sec. 4.3.

2.3 S_1 LQ

The $SU(2)_L$ singlet scalar LQ (S_1) gives another solution to the $R_{D^{(*)}}$ anomaly. The relevant Yukawa interactions with the SM fermions are described by

$$\begin{aligned}\mathcal{L}_{\mathrm{S_1LQ}} &= h_L^{ij}\overline{Q^C} i\tau_2 L_j \mathrm{S}_1 + h_R^{ij}\overline{u_i^C} P_R e_j \mathrm{S}_1 + \mathrm{h.c.} \\ &= \left[\left(V_{\mathrm{CKM}}^* h_L\right)^{ij}\overline{u_{Li}^C}\ell_{Lj} - h_L^{ij}\overline{d_{Li}^C}\nu_{Lj} + h_R^{ij}\overline{u_{Ri}^C}\ell_{Rj}\right]\mathrm{S}_1 + \mathrm{h.c.}\,.\end{aligned} \tag{10}$$

The contribution to the relevant WCs are given by

$$2\sqrt{2}G_F V_{cb} C_{V_1} = \frac{h_L^{33}\left(V_{\mathrm{CKM}}h_L^*\right)^{23}}{2M_{\mathrm{LQ}}^2}\,, \qquad 2\sqrt{2}G_F V_{cb} C_{S_2} = -\frac{h_L^{33}h_R^{*23}}{2M_{\mathrm{LQ}}^2}\,, \qquad C_{S_2} = -4C_T\,. \tag{11}$$

There are two sets of the WCs which are controlled by the different Yukawa couplings. Although the single C_{V_1} scenario looks promising, a stringent constraint from $b \to s\nu\overline{\nu}$ is unavoidable at the tree level. We will discuss the relevant constraints in Sec. 4 and Appendix B.

3 Event generation

Monte Carlo (MC) event generators are used to simulate both NP signal and SM background processes with a hard τ lepton and a large missing transverse momentum with/without an additional b-jet in the final states at $\sqrt{s} = 13$ TeV. The NP models are implemented via FEYNRULES v2.3.34 [54]. The model files are available in the arXiv web page. Event samples are generated by using MADGRAPH5_aMC@NLO v2.8.3.2 [55] interfaced with PYTHIA v8.303 [56] for hadronizations and decays of the partons. The MLM merging is adopted in the five-flavor scheme [57]. NNPDF2.3 in LHAPDF v6.3.0 [58] is used. Detector effects are simulated by using DELPHES v3.4.2 [59]. Here, we modified a prescription of the identification of the hadronic τ jet, as will be described below. The jets are reconstructed by using anti-k_T algorithm [60] with a radius parameter set to be $R = 0.5$. See Appendix A for some details.

To investigate the non-resonant $\tau\nu$ and $\tau\nu + b$ searches, and especially to evaluate an impact of the latter, the following two sets of kinematic cuts are compared:

cut a: Kinematic cuts to select the $\tau\nu$ events by following Ref. [34], originated from the CMS analysis [25]:

- 1. require exactly one τ-tagged jet, satisfying the transverse momentum of τ, $p_{\rm T}^{\tau} \geq 200$ GeV, and the pseudo-rapidity of τ, $|\eta_\tau| \leq 2.1$,
- 2. veto the event if it includes any isolated electron or muon with $p_{\rm T}^{e,\mu} \geq 20$ GeV within $|\eta_e| \leq 2.5$ or $|\eta_\mu| \leq 2.4$, where the lepton isolation criteria are the same as Ref. [34],
- 3. require large missing transverse momentum, $E_{\rm T}^{\rm miss} \geq 200$ GeV, to suppress the $W^{\pm}$ resonant contribution,
- 4. require that the missing momentum is balanced with the τ-tagged jet with the back-to-back configuration as $\Delta\phi(\vec{p}_{\rm T}^{\,\tau}, \vec{p}_{\rm T}^{\,\rm miss}) \geq 2.4$ and $0.7 \leq p_{\rm T}^{\tau}/E_{\rm T}^{\rm miss} \leq 1.3$ to further suppress the SM backgrounds.

cut b: Additional kinematic cuts to "**cut a**" for selecting the $\tau\nu + b$ events:

- 1. require exactly one b-tagged jet with $p_{\rm T}^{b} \geq 20$ GeV and $|\eta^b| < 2.5$.
- 2. restrict the number of light-flavored jets, $N_j \leq 2$, to suppress the top-decay related backgrounds, where the jets satisfy $p_{\rm T}^{j} \geq 20$ GeV and $|\eta^j| \leq 2.5$.

Energetic τ leptons can be emitted not only from the hard processes, but also from decays of energetic mesons, *e.g.*, $B \to \tau X$ (at a branching ratio $\sim 3\%$) and $D_s \to \tau X$ ($\sim 5\%$). Quantitatively, these secondary τ gives mild contributions to **cut a** and **cut b**. In reality, it is likely to be accompanied by nearby jets and vetoed by τ isolation conditions adopted in the ATLAS/CMS analyses.

Since they do not use cut-based analyses, an implementation of their isolation procedure is complicated and beyond the scope of this paper. In our analysis, events with τ whose parent particle is mesons or baryons are vetoed, for simplicity. Also, for a τ-tagging efficiency, the "VLoose" working point is adopted for the hadronic decays; $\varepsilon_{\tau\to\tau} = 0.7$ [61]. As the mis-tagging efficiencies, we apply $p_{\rm T}^j$-dependent efficiency based on Ref. [61]. For instance, $\varepsilon_{j\to\tau} = 3.7\times10^{-3}$ for $p_{\rm T}^j = 100$ GeV and 7.2×10^{-4} for $p_{\rm T}^j = 300$ GeV or larger. The mis-tagging rare $\varepsilon_{c,b\to\tau}$ is assumed to be 7.2×10^{-4} as a reference. When one imposes the condition requiring an additional b-jet in the final state, of crucial importance is which working point is chosen for the b-tagging efficiencies. For instance lower mis-tagging efficiencies can suppress backgrounds coming from fake b-jets. We adopt the following working point based on Table 4 of Ref. [62],

$$\varepsilon_{j\to b} = 1/1300\,, \qquad \varepsilon_{c\to b} = 1/27\,, \qquad \varepsilon_{b\to b} = 0.6\,. \tag{12}$$

Compared to the working point in Ref. [34],[#3] the mis-tagging rates, $\varepsilon_{j\to b}$ and $\varepsilon_{c\to b}$, are better by factors of 20 and 8, respectively, while the b-tagging rate $\varepsilon_{b\to b}$ is slightly worse. Therefore, it is expected that the number of background events originated from fake b-jets is reduced in our analysis for the **cut b** category.

Note that the charge of the final-state τ lepton is not distinguished in **cut a** or **cut b**, though it may be possible at the LHC as mentioned in Sec. 1 and will be discussed later. In order to stress this point, the searches are described with a script $\pm$ as "the $\tau^\pm\nu$ ($\tau^\pm\nu + b$) search" hereafter.

3.1 Background simulation

As for the SM background events generation, we basically trace the method explored in Ref. [34]. Nonetheless, since this is crucial to derive NP sensitivities, we dare to present all the essential steps in some details, though most of them may be familiar to experts. The six categories of the background processes are considered:

Wjj

The event simulations in MADGRAPH5_aMC@NLO are performed up to `QED=4`, which includes contributions from vector boson fusions. The W boson is assumed to decay as $W\to\tau\overline{\nu}$, and the events are matched allowing up to two jets. The Wjj contribution dominates the SM background in the **cut a** category, and also one of the main sources of the backgrounds for **cut b** because light-flavored jets are mis-tagged as b jets. The working point of b-tagging efficiencies is given in Eq. (12). It is checked that the number of events of W plus genuine b-jet is less than that of Wjj by more than three orders of magnitude for **cut b**. Therefore, improving the discrimination efficiency of the light-flavored jets from the genuine b jets can result in suppressing the SM background effectively.

Zjj

The Z boson is assumed to decay as $Z\to\nu\overline{\nu}$, contributing to missing transverse momentum. The events are matched allowing up to two jets. At least one fake τ-jet is necessary to pass **cut a**. Namely, the final state should include associated QCD jets. This channel gives the subdominant

[#3] The reference [34] adopted a different working point: $\varepsilon_{j\to b} = 0.015$, $\varepsilon_{c\to b} = 0.3$, and $\varepsilon_{b\to b} = 0.7$.

contribution both for **cut a** and **cut b**. Note that the ATLAS and CMS analyses categorize Zjj into "QCD jet," and estimate them with a data-driven technique, *e.g.*, extrapolating from Zjj with $Z \to \mu^+\mu^-$ events and requiring $p_{\rm T}^{\tau}/E_{\rm T}^{\rm miss} \leq 0.7$.

$t\bar{t}$

The top quarks are assumed to decay as $t\bar{t} \to bW^+\bar{b}W^-$ with both W bosons decaying to τ or one of them decaying to τ. The former contribution is larger by a factor of four than the latter after **cut a**, while both are of similar size after **cut b**.

Single t

The single top productions are divided by the following five sub-categories, $t+j$, $tW(1)$, $tW(2)$, $tZ(1)$, and $tZ(2)$. The top quark decays into bW, and the number in the parentheses expresses how many gauge bosons decay leptonically, *i.e.*, $W \to \tau\nu$ or $Z \to \nu\bar{\nu}$. More explicitly $t+j \to b\tau\nu j$ is categorized as $t+j$. $tW \to b\tau\nu jj$ and $tW \to b\tau\tau\nu\nu$ are classified into $tW(1)$ and $tW(2)$ respectively. $tZj \to b\tau\nu jjj$, $tZj \to b\tau\tau jjj$ and $tZj \to b\nu\nu jjj$ are denoted as $tZ(1)$, and $tZj \to b\tau\nu\tau\tau j$ and $tZj \to b\tau\nu\nu\nu j$ are classified into $tZ(2)$.

Z,γ Drell-Yan

A pair of τ leptons are produced via Drell-Yan processes mediated by Z or γ in accompany with up to two jets. Since the number of τ jets is required to be exactly one in **cut a**, another τ lepton needs to be missed in the detectors. Although the efficiency of τ mis-tagged as other particles is not so small, it is unlikely to achieve a large missing momentum because jets are rarely overlooked or their momenta are hardly mis-reconstructed so largely in the detectors. Thus, the contribution will be found to be negligibly small.

VV

Pair-productions of vector bosons are classified by the species as WW, $ZZ(\gamma)$, and $WZ(\gamma)$. The events for WW are simulated with both W's decaying to τ and allowing up to two additional jets or one of W's decaying into τ and allowing up to one additional jet. The $ZZ(\gamma)$ events involve those with one of Z's decaying as $Z \to \nu\bar{\nu}$ or into $\tau^+\tau^-$. As for $WZ(\gamma)$, the events are generated from a tauonic W decay along with $\gamma \to \tau^+\tau^-$ or $Z \to \tau^+\tau^-, \nu\bar{\nu}$. It will be shown that the resultant contribution is subdominant in **cut a** and of $\mathcal{O}(1)\%$ in **cut b**.

It is noted that pure QCD multi-jet backgrounds are not simulated in this paper. In order to pass **cut a/b**, one of energetic jets has to be mis-tagged as τ. Moreover, although another jet is required to be overlooked to pass the condition of large missing momentum, this rarely happens in the calorimeters. Here we assume that the contributions are negligible, for simplicity, though one needs full detector simulations for further studies. In fact, the CMS collaboration has checked that the QCD multi-jet background is smaller than that from Zjj in their simulation, and shown that the simulated result agrees with the data in a control region [25].

3.2 Signal simulation

Here, we show our setup with respect to the NP scenarios of interest for investigating the LHC sensitivities in the $\tau^{\pm}\nu(+b)$ search. Events of the NP signals are generated for each NP scenario by fixing the relevant LQ couplings and mass, and then matched by allowing up to two (five-flavored) jets. In turn, the couplings are encoded as in Eq. (4) to present our output. As the high-p_T tail is concerned, NP–SM interferences are tiny enough, *e.g.*, see Ref. [34] showing that the interference effect is a few percent level.[#4] Note that a possible s-channel production is also suppressed by the requirement of the back-to-back condition between τ and ν, see Appendix A. A set of process cards for the MADGRAPH event generation are available in the arXiv web page.

As already mentioned, we proceed with the LQ models that generate the effective four-fermion interactions at the EFT limit. Our approach has a benefit to clarify difference between EFT and a practical model of interest, especially for the case of the C_{V_1} type interaction as explained below.

Motivated by the $R_{D^{(*)}}$ anomaly, NP contributions to $b\bar{c} \to \tau\bar{\nu}$ have been studied in the EFT limit. However, one notices that there exist additional processes to be considered in realistic model setups. In fact, the V_1 operator is constructed from the U_1 LQ model, and C_{V_1} depends on the LQ couplings h_L^{23} and h_L^{33}, as seen in Eq. (6). Under the $SU(2)_L$ gauge invariance, the term, $\bar{Q}_L\gamma_\mu L_L U_1^\mu$, generates an interaction of $\bar{s}$–τ–U_1 as well as that of $\bar{c}$–ν_τ–U_1 in presence of h_L^{23}. Therefore, additional production processes such as $s\bar{c} \to \tau\bar{\nu}$ should be taken into account even in the EFT limit. In this paper, this new process is considered via the following effective Lagrangian,

$$\mathcal{L}_{\rm eff} \supset -2\sqrt{2}G_F V_{cb}\Big[(1+C_{V_1})(\bar{c}\gamma^\mu P_L b)(\bar{\tau}\gamma_\mu P_L \nu_\tau) + R_{s/b}C_{V_1}(\bar{c}\gamma^\mu P_L s)(\bar{\tau}\gamma_\mu P_L \nu_\tau)\Big] + \text{h.c.}. \tag{13}$$

The second term in the bracket corresponds to the new contribution, and $R_{s/b}$ is defined from Eq. (5) as

$$R_{s/b} \equiv \frac{|\text{coupling constant of } \bar{s}\text{–}\tau\text{–}U_1|}{|\text{coupling constant of } \bar{b}\text{–}\tau\text{–}U_1|} = \left|\frac{h_L^{23}}{h_L^{33}}\right|. \tag{14}$$

Hence, the U_1 LQ model possesses two parameters, $(C_{V_1}, R_{s/b})$, in the collider analysis, and the conventional EFT setup of V_1 is realized by taking $R_{s/b} \to 0$. Note that such an issue is not the case for the other operator scenarios. On the other hand, although the $\tau^{\pm}\nu + b$ search seems to be insensitive to it since the b quark is required in the final state, it will be shown that the $\bar{s}$–τ–U_1 interaction can affect the result through $gs \to c\tau\bar{\nu}$ with the final state b-jet mis-tagged from c-jet.

Single operator scenarios

Here, we list NP scenarios which can be responsible for the $R_{D^{(*)}}$ anomaly and whose collider signals will be investigated in this paper. First, from the view point of the EFT limit in Eq. (1), we consider LQ setups such that one of the WCs of C_{V_1}, C_{V_2}, C_{S_1}, C_{S_2}, and C_T is non-vanishing. Let us call this setup as "the single C_X scenario." Note that $R_{s/b} = 0$ is taken in the C_{V_1} scenario. The signal events are generated for the following LQ masses,

$$M_{\rm LQ} = \{1.5\,, 2.5\,, 4.0\,, 6.5\,, 10\,, 15\,, 20\}\ \text{TeV}. \tag{15}$$

[#4] When one considers dimension-eight effective interactions, it is found that its NP–SM interference contribution is further smaller than the dimension-six NP–SM interference [63].

According to Ref. [35] the EFT approximation becomes valid for $M_{\rm LQ} \gtrsim 10$ TeV in the $\tau^\pm\nu$ search. In this paper, $M_{\rm LQ}$ is taken up to 20 TeV to check the decoupling behavior in the $\tau^\pm\nu + b$ search. Then, we refer to the case of $M_{\rm LQ} = 20$ TeV as the EFT limit. It should be mentioned again that the LQ model which explains the $R_{D^{(*)}}$ anomaly is restricted as $M_{\rm LQ} < \mathcal{O}(10)$ TeV due to the perturbative unitarity bound [22].

The above LQ masses satisfy the constraints from the LQ direct searches. The searches have been performed by studying LQ pair-production channels at the ATLAS [64] (CMS [65]) $\int \mathcal{L}\,dt = 139\ \text{fb}^{-1}$ and provided limits on the LQ mass as $M_{\rm LQ} \geq 1.2\,(1.0)$ TeV for a scalar LQ, and $M_{\rm LQ} \geq 1.5\,(1.3)$ TeV for a gauged-vector LQ at the 95% CL. [#5] On the other hand, single-production channels can provide alternative bounds. However, since they depend on LQ couplings irrelevant to the $R_{D^{(*)}}$ anomaly, we do not take them into account.

As we focus on the NP interactions responsible for the $R_{D^{(*)}}$ anomaly, the other LQ couplings, which are irrelevant for $b \to c\tau\nu_\tau$, are set to be zero, and thus, the LQ production process comes only from the initial partons of cb, gc, gb, gg.

Single LQ scenarios

We also perform the analysis which is based on the LQ model rather than the EFT operator. In particular, multiple WCs can become non-vanishing simultaneously, or $R_{s/b}$ is not always zero. As aforementioned in Sec. 2, the following five scenarios can solve the $R_{D^{(*)}}$ anomaly by introducing a single LQ boson.

- The R_2 scalar LQ model induces the two independent WCs, $C_{V_2}(M_{\rm LQ})$ and $C_{S_2}(M_{\rm LQ}) = +4C_T(M_{\rm LQ})$, as given in Eq. (9). Thus, we study these two scenarios, called as single-$\text{R}_2(C_{V_2})$ and single-$\text{R}_2(C_{S_2})$ scenarios, respectively. Note that the former is identical to the C_{V_2} scenario (unlike C_{V_1} in the U_1 LQ scenario).

- The S_1 scalar LQ model induces the two independent WCs, $C_{V_1}(M_{\rm LQ})$ and $C_{S_2}(M_{\rm LQ}) = -4C_T(M_{\rm LQ})$, as seen in Eq. (11). In contrast to the R_2 LQ case, however, the single $C_{S_2} = -4C_T$ case cannot address the $R_{D^{(*)}}$ anomaly within $1\,\sigma$, though the tension can be relaxed. Thus, we investigate the scenario in a two-dimensional parameter space, (C_{V_1}, C_{S_2}), with assuming real WCs, simply called as S_1 LQ scenario.

- The U_1 vector LQ model possesses the two independent WCs, $C_{V_1}(M_{\rm LQ})$ and $C_{S_1}(M_{\rm LQ})$. In this paper, we investigate two scenarios in terms of the WCs of Eq. (6); the single C_{V_1} scenario assuming $C_{S_1} = 0$, and the scenario satisfying $C_{S_1} = -2e^{i\phi_R}C_{V_1}$ under the $U(2)$ flavor symmetry, as introduced in Sec. 2.1. Hereafter, they are referred as single-U_1 and $U(2)$-U_1 scenarios, respectively. One can easily find that the relative phase ϕ_R is almost irrelevant for the following collider analysis and taken to be zero. On the other hand, both two scenarios involve the aforementioned $R_{s/b}$. In our analysis, the region of $1/16 \leq R_{s/b} \leq 16$ is searched to see its effect in detail, in addition to the case of $R_{s/b} = 0$ that corresponds to the C_{V_1} scenario.

[#5] The lower bound for a strongly-coupled sector originated vector LQ is given as $M_{\rm LQ} \geq 1.7\,(1.6)$ TeV.

BG (**cut a**)	Wjj	$Zjj\,(Z\to\nu\bar{\nu})$	$t\bar{t}$	Z,γ DY	VV	single t	total
$0.7<m_{\rm T}<1$ TeV	70.5	20.1	0.34	3.03	1.30	0.02	95.3
$1\text{ TeV}<m_{\rm T}$	16.9	5.1	0.06	0.56	0.32	0.02	23.0
$1\text{ TeV}<m_{\rm T}$ [25]	22 ± 6.2	0.9 ± 0.5	<0.1	<0.1	0.7 ± 0.1	<0.1	23.4 ± 7.2
$1\text{ TeV}<m_{\rm T}$ [34]	18	5.2	0.44	0.0025	1.7	0.1	25.4

Table 1. Expected number of SM background events after **cut a** (the $\tau^{\pm}\nu$ search) for $\int\mathcal{L}dt=35.9\text{ fb}^{-1}$ and $\sqrt{s}=13$ TeV in each background category. The last two rows show the results obtained by Refs. [25] and [34]. Also shown are the total systematic uncertainties for the former. Detailed cut flows are shown in Table 9.

BG (**cut b**)	Wjj	$Zjj\,(Z\to\nu\bar{\nu})$	$t\bar{t}$	Z,γ DY	VV	single t	total
$0.7<m_{\rm T}<1$ TeV	0.58	0.37	0.056	0.28	0.018	0.029	1.33
$1\text{ TeV}<m_{\rm T}$	0.16	0.06	0.01	0.007	0.005	0.005	0.25
$1\text{ TeV}<m_{\rm T}$ [34]	0.18(5)	0.21(12)	0.29(3)	$4.2(4)\times10^{-5}$	0.35(5)	0.067(7)	1.10(14)

Table 2. Expected number of SM background events after **cut b** (the $\tau^{\pm}\nu+b$ search) for $\int\mathcal{L}dt=35.9\text{ fb}^{-1}$ and $\sqrt{s}=13$ TeV in each background category. The last row shows the result by Ref. [34], where a number in the parenthesis represents uncertainties. Note that their b-tagging efficiencies are different from ours (see the footnote #3). Detailed cut flows are shown in Table 10.

In the analysis, the LQ mass region in Eq. (15) is studied. Besides, since we are interested only in the LQ couplings relevant to the $R_{D^{(*)}}$ anomaly, the LQ production processes come from the initial partons of cb, gc, gb, gg for R_2 and S_1 LQs, while the additional production from cs is taken into account for U_1 LQ.

4 Numerical results

In this section, we present numerical results of the LHC simulations for the $\tau\nu(+b)$ processes. Also, it is argued how the requirement of an additional b-jet improves NP sensitivities and gives an impact on the NP solutions to the $R_{D^{(*)}}$ anomaly.

4.1 Event numbers after selection cuts

The expected numbers of SM background events after the cuts, **cut a** and **cut b**, are shown in Tables 1 and 2, respectively. They correspond to the result at the integrated luminosity of 35.9 fb^{-1} and $\sqrt{s}=13$ TeV, which is equivalent to the CMS result [25]. Note that we imposed a pre-cut given in Eq. (21) of Appendix A at the generator level in the analysis to reduce the simulation cost. The cut can affect the event distributions for $m_{\rm T}\lesssim500$ GeV, while the result is insensitive to it for $m_{\rm T}>700$ GeV. Detailed cut flows of the SM background are shown in Tables 9 and 10 in Appendix A.

From Table 1, it is found that the main background of **cut a** (specified for the $\tau^{\pm}\nu$ search, *i.e.*, without requiring b-jets in the final state) comes from the Wjj channel. Our result is consistent

signal (**cut a**)	$C_{V_1,1.5\,\mathrm{TeV}}$	$C_{V_1,\mathrm{EFT}}$	$C^{R_{s/b}=1}_{V_1,1.5\,\mathrm{TeV}}$	$C^{R_{s/b}=1}_{V_1,\mathrm{EFT}}$	$\mathrm{U}^{R_{s/b}=0}_{1,1.5\,\mathrm{TeV}}$	$\mathrm{U}^{R_{s/b}=0}_{1,\mathrm{EFT}}$	$\mathrm{U}^{R_{s/b}=1}_{1,1.5\,\mathrm{TeV}}$	$\mathrm{U}^{R_{s/b}=1}_{1,\mathrm{EFT}}$	BG
$0.7 < m_{\mathrm{T}} < 1$ TeV	90.0	139.4	225.9	351.4	361	582	502	809	95.3
1 TeV $< m_{\mathrm{T}}$	54.4	123.6	146.9	345.8	204	571	279	799	23.0

Table 3. Expected numbers of signal events after **cut a** (the $\tau^{\pm}\nu$ search) for $\int \mathcal{L}\,dt = 35.9\,\mathrm{fb}^{-1}$ and $\sqrt{s} =$ 13 TeV in the single C_{V_1} scenario (from second to fifth columns) and the $U(2)$-U_1 scenario ($C_{S_1} = -2\beta_R C_{V_1}$) (from sixth to ninth columns). In all cases, $C_{V_1} = 1$ is fixed, while the LQ mass is $M_{\mathrm{LQ}} = 1.5$ TeV or 20 TeV (the EFT limit). The s-quark contribution, parameterized by $R_{s/b}$, is also studied. The last column is the expected number of SM background (see Table 1). Detailed cut flows are shown in Tables 11 and 12.

signal (**cut b**)	$C_{V_1,1.5\,\mathrm{TeV}}$	$C_{V_1,\mathrm{EFT}}$	$C^{R_{s/b}=1}_{V_1,1.5\,\mathrm{TeV}}$	$C^{R_{s/b}=1}_{V_1,\mathrm{EFT}}$	$\mathrm{U}^{R_{s/b}=0}_{1,1.5\,\mathrm{TeV}}$	$\mathrm{U}^{R_{s/b}=0}_{1,\mathrm{EFT}}$	$\mathrm{U}^{R_{s/b}=1}_{1,1.5\,\mathrm{TeV}}$	$\mathrm{U}^{R_{s/b}=1}_{1,\mathrm{EFT}}$	BG
$0.7 < m_{\mathrm{T}} < 1$ TeV	11.6	16.6	13.9	21.7	53.9	86.4	55.8	92.0	1.33
1 TeV $< m_{\mathrm{T}}$	6.51	14.6	9.39	21.6	26.0	71.6	30.7	101	0.25

Table 4. Expected numbers of signal events after **cut b** (the $\tau^{\pm}\nu + b$ search) for $\int \mathcal{L}\,dt = 35.9\,\mathrm{fb}^{-1}$ and $\sqrt{s} = 13$ TeV. See the caption of Table 3 for further information. The last column is the expected number of SM background (see Table 2). Detailed cut flows are shown in Tables 13 and 14.

with those obtained by Refs. [25] and [34]. The next-to-leading contribution is provided by the Zjj channel and consistent with Ref. [34], while it is larger by a factor of 5 than the CMS result. Note that the CMS Zjj result is based on a data driven analysis. It should be mentioned that, although the background events are categorized by the channels, their criteria are not unique and not shown explicitly in the literature. Nevertheless, the total number of the SM background is consistent with those in Refs. [25] and [34] for $m_{\mathrm{T}} > 1$ TeV, which may validate our analysis.

Let us comment on a preliminary result of the $\tau^{\pm}\nu$ search by the ATLAS collaboration with $\int \mathcal{L}\,dt = 139\,\mathrm{fb}^{-1}$ [26]. It has not observed any significant excess, and hence, constrained the W' mass as $\gtrsim 5$ TeV. To be precise, the observed event number is smaller than the expected SM background, and thus, one can infer (much) stronger upper bounds on the EFT operators in Eq. (9) than the results based on the CMS analysis. Nevertheless, our result cannot be compared with it straightforwardly because the ATLAS has not provided enough information for this purpose and the tagging efficiency of hadronic τ is different from ours.

In Table 2, an additional b-jet is required, corresponding to **cut b** (specified for the $\tau^{\pm}\nu + b$ search). It is shown that the total number of the background is suppressed by about two orders of magnitude versus the result for **cut a**. In detail, the event number after the cut decreases in every channel, particularly in Wjj and Zjj. Here, the range of reduction depends on whether the event involves genuine b-jets or not. Also, it is noticed from Table 10 that the condition on the number of b-jets is effective to suppress the background when it does not come from the top quarks, while the back-to-back condition reduces those via the top quarks. Our result is also compared with that given by Ref. [34], where the b-tagging efficiencies, especially those for fake b-jets, are different from ours (see the footnote #3). The total number of the background becomes smaller by $\sim 40\%$ than their result. The difference is prominent in Zjj, $t\bar{t}$ and VV, because a large number of events include fake b-jets.

The expected numbers of signal events after the selections, **cut a** and **cut b**, are shown in

Tables 3 and 4, respectively. As a reference, the single C_{V_1} scenario and the $U(2)$-U_1 scenario ($C_{S_1} = -2\beta_R C_{V_1}$) are evaluated at $\int \mathcal{L}\,dt = 35.9\,\text{fb}^{-1}$ and $\sqrt{s} = 13$ TeV. Here, $C_{V_1} = 1$ is fixed, while the LQ mass is set to be $M_{\text{LQ}} = 1.5$ TeV and 20 TeV, where the latter corresponds to the EFT limit. By varying $R_{s/b}$, effects of the s-quark contribution are also studied. Detailed cut flows for those scenarios are given in Tables 11, 12, 13, and 14 of Appendix A.

From the tables, it is confirmed that the event number after the cut depends on the LQ mass for $M_{\text{LQ}} = \mathcal{O}(1)$ TeV. For instance, according to the results for $m_{\text{T}} > 1$ TeV the event number with $C_{V_1,1.5\,\text{TeV}} = 1$ is less than a half of that in the EFT limit, $C_{V_1,\text{EFT}} = 1$. Such a feature is valid for both **cut a** and **cut b**.

Let us comment that the signal event numbers in our results are smaller than those in Ref. [34], *e.g.*, 25.6 events are expected for $C_{V_1,\text{EFT}}$ ($m_{\text{T}} > 1$ TeV) in their analysis. This is mainly because the b mis-tagging rate is different; $\varepsilon_{c\to b} = 0.3$ in Ref. [34], while it is $1/27 \simeq 0.04$ in our case. With their set up, we checked that almost a half of the signal events come from this fake b-jet in the simulation.

4.2 Test of background-only hypothesis

In order to study sensitivities to the NP contributions, the background-only hypothesis is tested; under the hypothesis, the result is identified to be consistent with the SM if the total number of events, *i.e.*, the sum of the signal and background event numbers (denoted as N_{Sig} and N_{BG}, respectively), is smaller than an upper bound (U_{tot}). In this paper, the bound is determined as follows. Let us first turn off the systematic uncertainty to focus on the statistical one. Under the background-only hypothesis, U_{tot} satisfies the relation,

$$\sum_{n=0}^{N_{BG}} P(n; U_{\text{tot}}^{\text{stat}}) = p\,, \tag{16}$$

where $P(n;\mu)$ is the probability function of the Poisson distribution for observing n events with the mean value μ, and $p = 0.05$ is taken, corresponding to 95% confidence level (CL). Here, U_{tot} is denoted with the superscript "stat," since the systematic uncertainty is ignored. Then, the systematic uncertainty is taken into account. Although it is unknown, we assign 60% relative to the mean value at 95% CL for $\int \mathcal{L}\,dt = 35.9\,\text{fb}^{-1}$ as inferred from the CMS result [25].[#6] Furthermore, it is supposed to be scaled with $1/\sqrt{L}$ for the integrated luminosity L. Hence, the systematic uncertainty is assigned as $\sigma_{\text{syst}}^{95\%} = N_{BG} \times 60\% \times \sqrt{35.9\,[\text{fb}]/L\,[\text{fb}]}$. In this paper, we combine the systematic uncertainty with the statistical one linearly, and then, U_{tot} is obtained as $U_{\text{tot}} = U_{\text{tot}}^{\text{stat}} + \sigma_{\text{syst}}^{95\%}$. Finally, the upper bound on the NP signal event number N_{Sig} is derived as $S^{95\%} = U_{\text{tot}} - N_{BG}$; the result is regarded as the SM consistent if $N_{Sig} < S^{95\%}$ is satisfied.

In the analysis, the expected number of events is not always integers, as shown in the tables of the previous subsection. Then, N_{BG} in Eq. (16) is replaced with $\lfloor N_{BG} \rfloor$ corresponding to the mode for the Poisson distribution. Here, $\lfloor x \rfloor$ is the floor function, *i.e.*, returns the maximum integer not exceeding x. The background event number for $\int \mathcal{L}\,dt = 35.9\,\text{fb}^{-1}$ is given in Tables 1 and 2. For higher luminosity, the event numbers are obtained by scaling the results in the tables with

[#6] As shown in Table 1, the SM background is dominated by Wjj. The CMS analysis obtains the total systematic uncertainty of 28% on this channel at 68% CL [25].

corresponding to the integrated luminosity. Note that, although the HL-LHC (LHC Run 4 and 5) will be operated at $\sqrt{s} = 14$ TeV, we ignore differences between the results at $\sqrt{s} = 13$ and 14 TeV, for simplicity.

Before proceeding to the results, let us mention about the $m_{\rm T}$ dependence of the NP sensitivities. From the tables it can be found that the category of $m_{\rm T} > 1$ TeV provides higher sensitivities to the NP contributions than the category of $0.7 < m_{\rm T} < 1$ TeV. Similarly, among the three different $m_{\rm T}$ bins in the CMS analysis, $m_{\rm T} < 500$ GeV, 500 GeV $< m_{\rm T} < 1$ TeV and $m_{\rm T} > 1$ TeV, the last one provides the most stringent constraints. Hence, we will present the results obtained from $m_{\rm T} > 1$ TeV in the following.

4.3 Single operator scenarios

In Tables 5 and 6, the expected sensitivities to $|C_X(\Lambda_{\rm LHC})|$ are shown for each single operator scenario in the $\tau^\pm\nu$ and $\tau^\pm\nu + b$ searches, respectively. They are determined from $S^{95\%}$ defined in the previous subsection. The number without (inside) the parenthesis is obtained in the EFT limit (at $M_{\rm LQ} = 1.5$ TeV). The integrated luminosities are $\int \mathcal{L}\,dt = 139$ fb^{-1} (for the current sensitivity) and 1000/3000 fb^{-1} (for future). The results are provided at two scales; one is a scale of flavor experiments, $m_b = 4.2$ GeV, and another is that of the collider search, $\Lambda_{\rm LHC}$, which is fixed to be 1 TeV in this paper. The WCs at the scale of $m_b = 4.2$ GeV are derived by taking RG running corrections into account. For the $\tau^\pm\nu$ search, the current upper bounds on $|C_X(m_b)|$ are also listed in Table 5. They are obtained in Ref. [35] based on the CMS result with $\int \mathcal{L}\,dt = 35.9$ fb^{-1} [25]. Similar limits are provided in Refs. [30, 34]. It is noted that there are no experimental studies in the $\tau^\pm\nu + b$ search.

The LQ mass dependence of the sensitivities are shown in Fig. 1 for the integrated luminosities of $\int \mathcal{L}\,dt = 139$ (solid line) and 3000 fb^{-1} (dashed). The scale is set to be $\Lambda_{\rm LHC}$. The blue (red) lines correspond to the $\tau^\pm\nu$ ($\tau^\pm\nu + b$) search. In the figure, the upper plot for each scenario shows a sensitivity to the WC based on **cut a** or **cut b**.

As mentioned above, the charge of the final-state τ lepton is not identified in **cut a** or **cut b**. If the event selections are performed with distinguishing the τ-lepton charge, the sensitivities may be affected. The lower plot in each scenario displays $\delta C_X^{95\%}/C_X^{95\%}|_{\tau^\pm}$ for $\int \mathcal{L}\,dt = 3000$ fb^{-1} with $\delta C_X^{95\%} = C_X^{95\%}|_{\tau^\pm} - C_X^{95\%}|_{\tau^-}$, where $C_X^{95\%}|_{\tau^{-(\pm)}}$ is the sensitivity to the WC with (without) selecting negative charged τ leptons, τ^-. A positive value means that the sensitivities are improved by selecting τ^- versus the result collecting both τ^+ and τ^-.

Let us summarize our observations from the figure and tables:

- In the $\tau^\pm\nu$ search, compared with the current bounds, some of the sensitivities are not improved even with the larger dataset of $\int \mathcal{L}\,dt = 139$ fb^{-1}. This is mainly because the observed data at CMS in Ref. [25] are smaller than the expected SM background, probably due to unexpected (statistical) fluctuations.

- In the $\tau^\pm\nu$ search, the sensitivities to the WCs can be improved by a factor of two at $\int \mathcal{L}\,dt =$ 3000 fb^{-1} compared with the current bounds (36 fb^{-1}) or sensitivities (139 fb^{-1}).

- By requiring an additional b-jet in the final states, the NP sensitivities can be improved by $\approx 40\%$ versus those in the $\tau^\pm\nu$ search. Note that this is beyond the statistical uncertainty

$\tau^{\pm}\nu$ search	C_{V_1}	C_{V_2}	C_{S_1}	C_{S_2}	C_T
current upper bound on EFT [35]: LHC 36 fb^{-1}					
$\mu = m_b$	0.32	0.33	0.55	0.55	0.17
sensitivity: LHC 139 fb^{-1}					
$\mu = \Lambda_{\rm LHC}$	0.30 (0.46)	0.32 (0.68)	0.32 (0.54)	0.32 (0.59)	0.18 (0.46)
$\mu = m_b$	0.30 (0.46)	0.32 (0.68)	0.55 (0.93)	0.55 (1.02)	0.15 (0.39)
sensitivity: HL-LHC 1000 fb^{-1}					
$\mu = \Lambda_{\rm LHC}$	0.18 (0.28)	0.20 (0.41)	0.19 (0.33)	0.19 (0.35)	0.11 (0.28)
$\mu = m_b$	0.18 (0.28)	0.20 (0.41)	0.33 (0.56)	0.33 (0.61)	0.09 (0.24)
sensitivity: HL-LHC 3000 fb^{-1}					
$\mu = \Lambda_{\rm LHC}$	0.14 (0.21)	0.15 (0.31)	0.15 (0.25)	0.15 (0.27)	0.08 (0.21)
$\mu = m_b$	0.14 (0.21)	0.15 (0.31)	0.25 (0.43)	0.25 (0.47)	0.07 (0.18)

Table 5. Expected sensitivities to the absolute value of the WCs in the single-operator scenarios. They are evaluated at the scale of $\mu = \Lambda_{\rm LHC}$ and m_b based on **cut a** (the $\tau^{\pm}\nu$ search). The number without (inside) the parenthesis correspond to the EFT limit ($M_{\rm LQ} = 1.5$ TeV). Also shown are the current upper bounds [35] based on the dataset of CMS 35.9 fb^{-1} [25].

$\tau^{\pm}\nu + b$ search	C_{V_1}	C_{V_2}	C_{S_1}	C_{S_2}	C_T
sensitivity: LHC 139 fb^{-1}					
$\mu = \Lambda_{\rm LHC}$	0.20 (0.31)	0.20 (0.41)	0.20 (0.33)	0.18(0.32)	0.11 (0.22)
$\mu = m_b$	0.20 (0.31)	0.20 (0.41)	0.33 (0.57)	0.31 (0.56)	0.09 (0.19)
sensitivity: HL-LHC 1000 fb^{-1}					
$\mu = \Lambda_{\rm LHC}$	0.12 (0.18)	0.12 (0.24)	0.11 (0.20)	0.11 (0.19)	0.06 (0.13)
$\mu = m_b$	0.12 (0.18)	0.12 (0.24)	0.20 (0.34)	0.18 (0.33)	0.05 (0.11)
sensitivity: HL-LHC 3000 fb^{-1}					
$\mu = \Lambda_{\rm LHC}$	0.09 (0.14)	0.09 (0.18)	0.09 (0.15)	0.08 (0.14)	0.05 (0.10)
$\mu = m_b$	0.09 (0.14)	0.09 (0.18)	0.15 (0.26)	0.14 (0.25)	0.04 (0.08)

Table 6. Same as Table 5 but for **cut b** (the $\tau^{\pm}\nu + b$ search).

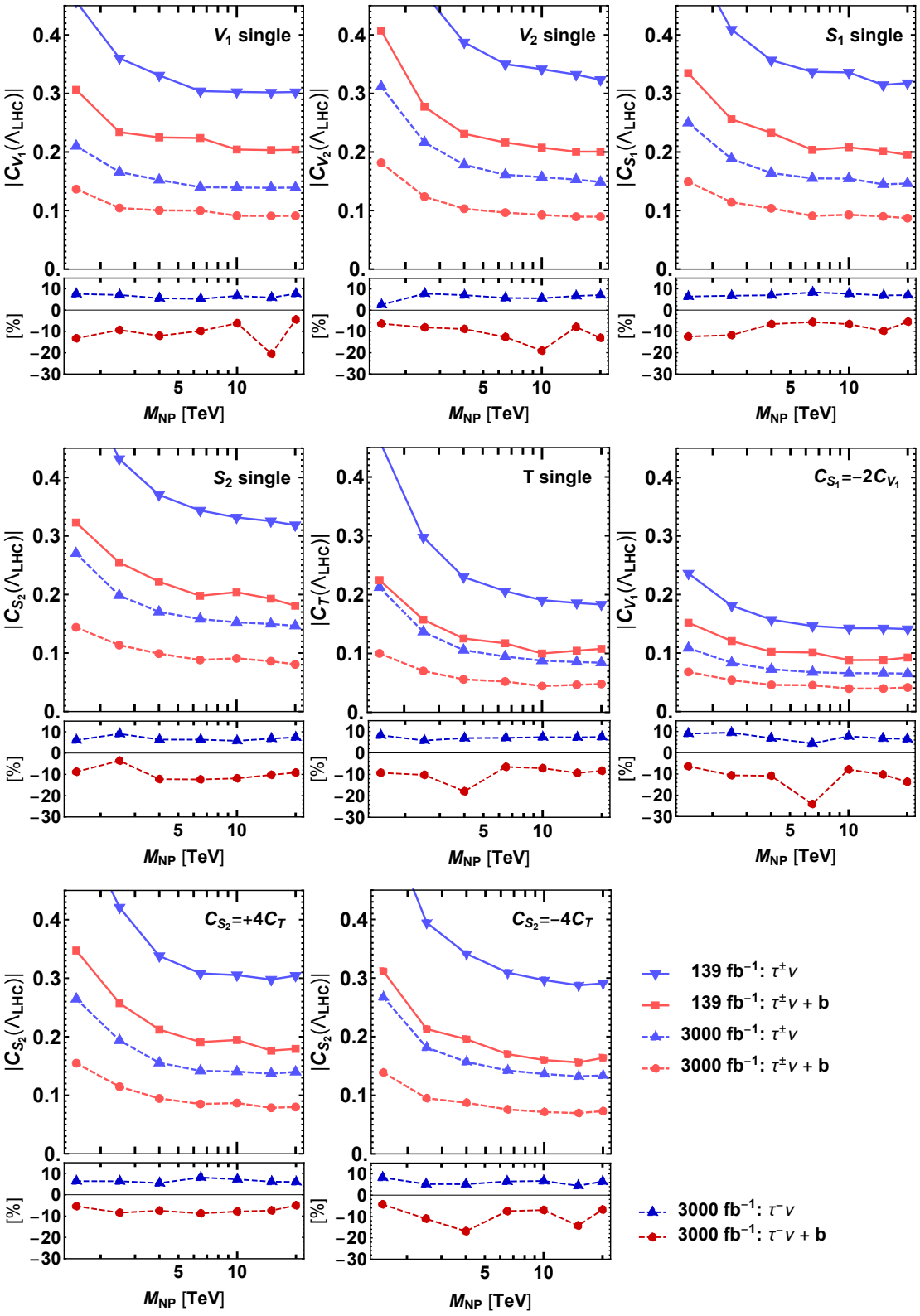

Figure 1. Expected sensitivities to the absolute value of $C_X(\Lambda_{\rm LHC})$ (upper in each scenario) with $\int \mathcal{L}\,dt =$ 139 fb^{-1} (solid) and 3000 fb^{-1} (dashed) in the $\tau^{\pm}\nu$ (blue) and $\tau^{\pm}\nu + b$ (red) searches. In the lower plot of each scenario, $\delta C_X^{95\%}/C_X^{95\%}|_{\tau^{\pm}}$ is displayed for $\int \mathcal{L}\,dt = 3000$ fb^{-1} with $\delta C_X^{95\%} = C_X^{95\%}|_{\tau^{\pm}} - C_X^{95\%}|_{\tau^{-}}$, where $C_X^{95\%}|_{\tau^{-(\pm)}}$ is the sensitivity to the WC with (without) selecting τ^{-}.

of our MC; in the analysis, we generate 100K events for each NP model point, and the number of signal events after the cut could become $\lesssim 100$ for $\tau^- \nu + b$, leading to $\mathcal{O}(10)\%$ MC-uncertainty at most.

- The sensitivities depend on the LQ mass obviously; they become better as the mass increases. The dependence for $\tau^\pm \nu + b$ is similar to that for $\tau^\pm \nu$. It is found that the sensitivity from the $\tau^\pm \nu + b$ search is better than that from $\tau^\pm \nu$ in the whole mass region. (Note that the conclusion is valid for $R_{s/b} \lesssim 1$. See Fig. 5.)

- In the case of the $\tau^- \nu$ search, by selecting the negative-charged τ leptons, the sensitivities can be improved by $\approx 10\%$ compared with the result obtained without selecting τ^-. However, the selection is not effective to improve the sensitivity for $\tau^- \nu + b$, especially because the number of events after the cut is not large enough even at $\int \mathcal{L}\, dt = 3000\ \text{fb}^{-1}$; the number of signal events is halved by the charge selection. Then, with the number of background events $N_{BG} = \mathcal{O}(10)$, the reduction of N_{BG} due to the charge selection is not sufficient for improving U_{tot}. In other words, we found that larger N_{BG} or better reduction is necessary to improve the sensitivity.

- In small LQ mass regions, the sensitivity for C_{V_1} is better than that for C_{V_2} at $\int \mathcal{L}\, dt = 3000\ \text{fb}^{-1}$, because of differences of τ angular distributions; the signal acceptance for the former is better than that for the latter (see Ref. [35]).

4.4 Single LQ scenarios

We discuss an impact of the LHC searches on the single LQ scenarios that can solve the $R_{D^{(*)}}$ anomaly. There are three single LQ fields, U_1, R_2, and S_1, introduced in Secs. 2.1, 2.2, and 2.3, respectively. For calculating the flavor observables such as $R_{D^{(*)}}$, we used the formulae of Ref. [39] with updating the form factors [11].

Let us first summarize the expected sensitivities based on the $\tau^\pm \nu$ and $\tau^\pm \nu + b$ searches in Tables 7 and 8, respectively. Here, the sensitivity to C_{S_2} is shown for R_2 and S_1, while that to C_{S_1} is given for the scenario of U_1 LQ with $U(2)$ flavor symmetry. The interplay with the $R_{D^{(*)}}$ anomaly is discussed in the following subsections.

In discussing the LHC search for the NP contributions and its interplay with the flavor observables, there are three renormalization scales; $\mu = m_b$, Λ_{LHC}, and M_{LQ}. The WCs in different energy scales should be evaluated by taking the RG corrections into account [13, 66, 67]. Although all WCs are to be input at $\mu = M_{\text{LQ}}$, we show the results with discarding the RG corrections between $\Lambda_{\text{LHC}} = 1$ TeV and $M_{\text{LQ}} = \mathcal{O}(1)$ TeV, because they are found to be negligible (a few percent level for WCs). Nonetheless, the corrections are taken into account for $\mu = m_b$.

4.4.1 R_2 LQ scenarios

In the R_2 LQ model, two sets of WCs, $C_{V_2}(M_{\text{LQ}})$ and $C_{S_2}(M_{\text{LQ}}) = +4C_T(M_{\text{LQ}})$, are induced independently, as explained in Eq. (9). Thus, we study the following two scenarios; single-$\text{R}_2(C_{V_2})$ and single-$\text{R}_2(C_{S_2})$ scenarios separately. For each scenario, in order to solve the $R_{D^{(*)}}$ anomaly, we obtain that the WCs are favored to be

$$\text{single-R}_2(C_{V_2}) : C_{V_2}(\Lambda_{\text{LHC}}) \approx \pm i 0.42\,, \quad \text{single-R}_2(C_{S_2}) : C_{S_2}(\Lambda_{\text{LHC}}) \approx -0.07 \pm i 0.35\,, \tag{17}$$

$\tau^{\pm}\nu$ search	$R_2(C_{S_2})$	$S_1(C_{S_2})$	$U_1^{R_{s/b}=0}(C_{S_1})$	$U_1^{R_{s/b}=1}(C_{S_1})$	$C_{V_1}^{R_{s/b}=1}$
sensitivity: LHC 139 fb^{-1}					
$\mu = \Lambda_{\rm LHC}$	0.30 (0.58)	0.29 (0.58)	0.28 (0.47)	0.24 (0.40)	0.18 (0.28)
$\mu = m_b$	0.51 (0.96)	0.52 (1.04)	0.48 (0.81)	0.41 (0.69)	0.18 (0.28)
sensitivity: HL-LHC 1000 fb^{-1}					
$\mu = \Lambda_{\rm LHC}$	0.18 (0.35)	0.18 (0.35)	0.17 (0.28)	0.14 (0.24)	0.11 (0.17)
$\mu = m_b$	0.31 (0.58)	0.32 (0.63)	0.29 (0.49)	0.25 (0.42)	0.11 (0.17)
sensitivity: HL-LHC 3000 fb^{-1}					
$\mu = \Lambda_{\rm LHC}$	0.14 (0.26)	0.13 (0.27)	0.13 (0.22)	0.11 (0.19)	0.08 (0.13)
$\mu = m_b$	0.23 (0.44)	0.24 (0.48)	0.22 (0.37)	0.19 (0.32)	0.08 (0.13)

Table 7. Expected sensitivities of the absolute value of the WCs for **cut a** in the single LQ scenarios. The sensitivity to C_{S_2} is shown for R_2 and S_1, while that to C_{S_1} is given for the scenario of U_1 LQ with $U(2)$ flavor symmetry. See Table 5 for details of the descriptions.

$\tau^{\pm}\nu + b$ search	$R_2(C_{S_2})$	$S_1(C_{S_2})$	$U_1^{R_{s/b}=0}(C_{S_1})$	$U_1^{R_{s/b}=1}(C_{S_1})$	$C_{V_1}^{R_{s/b}=1}$
sensitivity: LHC 139 fb^{-1}					
$\mu = \Lambda_{\rm LHC}$	0.18 (0.35)	0.16 (0.31)	0.18 (0.30)	0.16 (0.28)	0.17 (0.25)
$\mu = m_b$	0.30 (0.58)	0.29 (0.56)	0.32 (0.52)	0.27 (0.48)	0.17 (0.25)
sensitivity: HL-LHC 1000 fb^{-1}					
$\mu = \Lambda_{\rm LHC}$	0.11 (0.20)	0.10 (0.18)	0.11 (0.18)	0.09 (0.17)	0.10 (0.15)
$\mu = m_b$	0.18 (0.34)	0.17 (0.33)	0.19 (0.31)	0.16 (0.28)	0.10 (0.15)
sensitivity: HL-LHC 3000 fb^{-1}					
$\mu = \Lambda_{\rm LHC}$	0.08 (0.15)	0.07 (0.14)	0.08 (0.14)	0.07 (0.13)	0.07 (0.11)
$\mu = m_b$	0.13 (0.26)	0.13 (0.25)	0.14 (0.23)	0.12 (0.21)	0.07 (0.11)

Table 8. Same as Table 7 but for **cut b** (the $\tau^{\pm}\nu + b$ search).

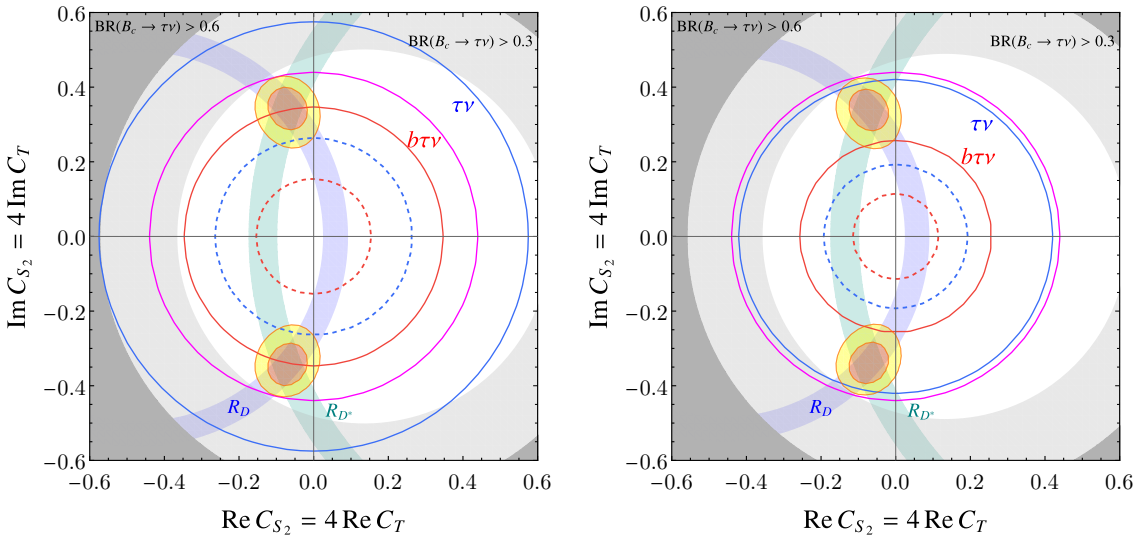

(a) $M_{\mathrm{R_2\,LQ}} = 1.5$ TeV (b) $M_{\mathrm{R_2\,LQ}} = 2.5$ TeV

Figure 2. The $\mathrm{R_2}$ LQ scenario with $M_{\mathrm{LQ}} = 1.5$ and 2.5 TeV. The regions outside the blue and red lines are probed by the $\tau^\pm\nu$ and $\tau^\pm\nu + b$ searches, respectively, where the solid (dashed) lines correspond to $\int \mathcal{L}\,dt = 139\ \mathrm{fb}^{-1}$ ($3000\ \mathrm{fb}^{-1}$). The magenta line shows the current bound from the experimental data with $\int \mathcal{L}\,dt = 36\ \mathrm{fb}^{-1}$ [35]. The (lighter) gray shaded regions are constrained by $\mathrm{BR}(B_c \to \tau\nu) > 0.6$ (> 0.3). The R_D and R_{D^*} anomalies are explained at $1\,\sigma$ in the blue and green shaded regions, respectively, while the combined fit at $1/2\,\sigma$ is shown in orange/yellow.

where the measured values of R_D and R_{D^*} are fitted. Note that $\pm$ does not mean an uncertainty but represents two solutions. Since the LHC study is almost insensitive to the phase of WCs, it is set to be zero in the collider analysis.

Such large WCs are expected to be probed at the LHC.[#7] In the single-$\mathrm{R_2}(C_{V_2})$ scenario, by comparing Tables 7 and 8 with the background results in Fig. 1, it is found that the LHC sensitivity of the $\tau^\pm\nu$ search is marginal at $\int \mathcal{L}\,dt = 139\ \mathrm{fb}^{-1}$ to test the $R_{D^{(*)}}$ explanation depending on the LQ mass, whereas that of the $\tau^\pm\nu + b$ search is enough to probe the parameter region in all ranges of the LQ mass. We would like to stress that the scenario can be probed with use of the current data samples at the LHC ($139\ \mathrm{fb}^{-1}$) for $\tau^\pm\nu + b$. On the other hand, in the single-$\mathrm{R_2}(C_{S_2})$ scenario, it is also shown that the $R_{D^{(*)}}$-favored value of $|C_{S_2}(\Lambda_{\mathrm{LHC}})| \approx 0.36$ can be fully probed by the $\tau^\pm\nu + b$ search at $139\ \mathrm{fb}^{-1}$, but not by $\tau^\pm\nu$. Therefore, it is concluded that requiring an additional b-jet is significant to test the LQ scenarios in light of the the $R_{D^{(*)}}$ anomaly.

The combined summary plot for the LHC sensitivity and the allowed region from the flavor observables is shown in Fig. 2 for the case of the single-$\mathrm{R_2}(C_{S_2})$ scenario with $M_{\mathrm{LQ}} = 1.5$ TeV and 2.5 TeV. The sensitivity at $\int \mathcal{L}\,dt = 139\ \mathrm{fb}^{-1}$ from the $\tau^\pm\nu$ and $\tau^\pm\nu + b$ channels are denoted by solid blue and red lines, respectively. Their HL-LHC prospects at $\int \mathcal{L}\,dt = 3000\ \mathrm{fb}^{-1}$ are shown

[#7] Interference with the SM part is preferred to be small by a fit for the $R_{D^{(*)}}$ anomaly in the $\mathrm{R_2}$ LQ model. Therefore, resultant WCs have large imaginary components, and their absolute values tend to be large enough to be able to probed at the LHC.

in dashed lines with the same color. The magenta lines are the current constraint from the CMS 36 fb^{-1} data, taken from Ref. [35] assuming $M_{\rm LQ} = 2$ TeV. The blue and green bands show the region favored by the measured R_D and R_{D^*}, respectively. Then, the combined $1\,\sigma$ ($2\,\sigma$) regions are shown in red (yellow). We also put the B_c constraint as ${\rm BR}(B_c \to \tau\nu) < 60\%$ (30%) shown in (light) gray as references. Here, an updated study for the $B_c \to \tau\nu$ constraint is available in Refs. [68, 69]. We can clearly check from this figure that the $\tau^\pm\nu + b$ search fully (partially) covers the single-R$_2$(C_{S_2}) scenario with $M_{\rm LQ} > 2.5$ TeV (1.5 TeV $< M_{\rm LQ} <$ 2.5 TeV) responsible for the $R_{D^{(*)}}$ anomaly.

4.4.2 S$_1$ LQ scenario

In the S$_1$ LQ model, two sets of WCs, $C_{V_1}(M_{\rm LQ})$ and $C_{S_2}(M_{\rm LQ}) = -4C_T(M_{\rm LQ})$, are induced independently as given in Eq. (11). In the latter case, although the $R_{D^{(*)}}$ discrepancy can be reduced, the experimental result cannot be addressed within $1\,\sigma$. Thus, the study is performed in the two-dimensional parameter space, (C_{V_1}, C_{S_2}).

In Fig. 3, the LHC sensitivity and the region favored by the $R_{D^{(*)}}$ anomaly are shown for the S$_1$ LQ scenario on the plane of (C_{V_1}, C_{S_2}). Here, the imaginary components are fixed to be zero. See Fig. 2 for the color convention. As briefly mentioned in Sec. 2.3, unlike the cases for R$_2$ and U$_1$ LQs, the S$_1$ LQ scenario inevitably produces a tree-level contribution to $b \to s\nu\overline{\nu}$ in addressing $R_{D^{(*)}}$. Thus, the parameter space is constrained from precision measurements of $B \to K^{(*)}\nu\overline{\nu}$, which is shown in the figure with the cyan-shaded region. Its evaluation formula is given in Appendix B. In addition, a more robust flavor bound comes from the B_s–$\bar{B}_s$ mixing (ΔM_s). Based on the studies of Refs. [70, 71], the ΔM_s constraint is provided in the figure with the red-shaded region. This bound is comparable to or severer than $B \to K^{(*)}\nu\overline{\nu}$ depending on the LQ mass. See again Appendix B for its detail. Although $\Delta M_d/\Delta M_s$ can give more stringent bound in general since QCD uncertainties are partially canceled, this constraint is avoidable if additional LQ contributions to ΔM_d are introduced properly.

From the figure, we see that the S$_1$ LQ mass larger than 4 TeV is disfavored by the ΔM_s and $B \to K^{(*)}\nu\overline{\nu}$ constraints. Since this implies that the smaller LQ mass $M_{\rm LQ} < 4$ TeV is viable for the $R_{D^{(*)}}$ anomaly, the LQ mass dependence on the NP sensitivity of the present LHC searches is important. Then, one can see that the $\tau^\pm\nu + b$ search at $\int \mathcal{L}\,dt = 3000$ fb^{-1} can reach the sensitivity to probe this scenario, while $\tau^\pm\nu$ cannot.

4.4.3 U$_1$ LQ scenarios

The U$_1$ vector LQ model introduced in Sec. 2.1 is one of the most promising candidates to solve the B anomalies. In fact, unlike the above two scalar LQ scenarios, flavor constraints can be suppressed or avoided. Therefore, the LHC search is significant to probe the model. In this paper, we investigate two scenarios in terms of the WCs of Eq. (6); the single C_{V_1} scenario (setting $C_{S_1} = 0$), and the scenario satisfying $C_{S_1} = -2e^{i\phi_R}C_{V_1}$ with the $U(2)$ flavor symmetry, referred as the single-U$_1$ and $U(2)$-U$_1$ scenarios, respectively. By performing a parameter fit for these two scenarios to the $R_{D^{(*)}}$ measurement, we obtain the following WCs,

$$\text{single-U}_1 : C_{V_1}(\Lambda_{\rm LHC}) \approx 0.09\,, \qquad U(2)\text{-U}_1 : C_{V_1}(\Lambda_{\rm LHC}) \approx 0.09\,,\ \phi_R \approx \pm 0.42\pi\,. \tag{18}$$

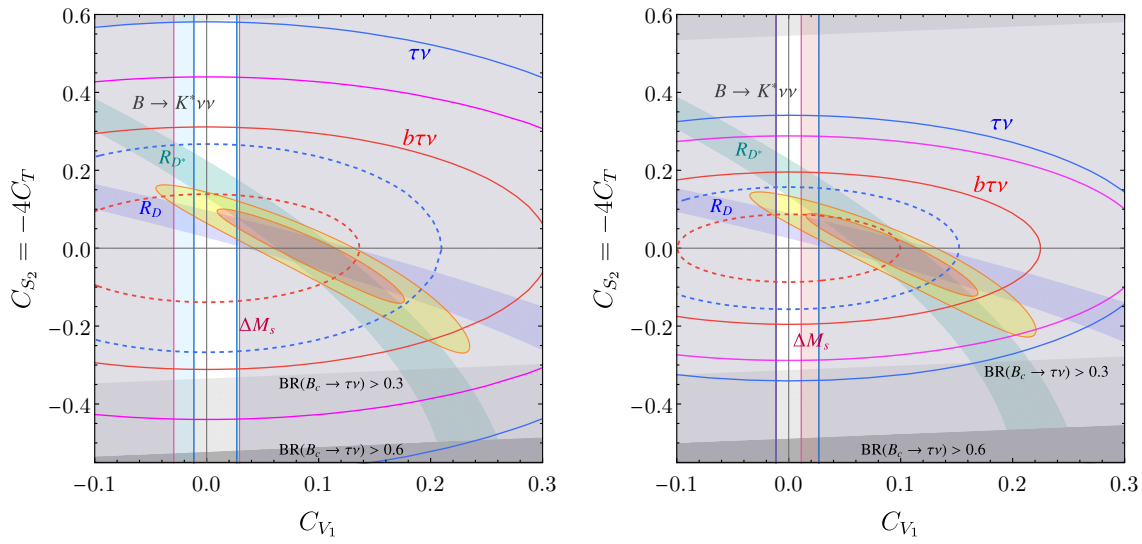

(a) $M_{\mathrm{S_1\,LQ}} = 1.5$ TeV (b) $M_{\mathrm{S_1\,LQ}} = 4.0$ TeV

Figure 3. The S_1 LQ scenario with $M_{\mathrm{LQ}} = 1.5$ TeV and 4.0 TeV on the (C_{V_1}, C_{S_2}) plane. The color convention is the same as in Fig. 2. The magenta lines are the current bound from the experimental data with $\int \mathcal{L}\,dt = 36$ fb^{-1} by assuming $M_{\mathrm{LQ}} = 2$ TeV (left panel) and the EFT limit (right panel) [35]. In addition, the cyan-shaded region is excluded by the $B \to K^* \nu\overline{\nu}$ measurement at the 90% CL, and the red-shaded region is excluded by ΔM_s.

Note again that $\pm$ does not mean an uncertainty. Also, the phase ϕ_R for $U(2)$-$\mathrm{U_1}$ is almost irrelevant for the present LHC study.

In Fig. 4, the NP sensitivities are shown in the $\tau^\pm\nu$ ($\tau^\pm\nu + b$) search by the blue (red) lines. The solid (dashed) lines correspond to $\int \mathcal{L}\,dt = 139$ fb^{-1} (3000 fb^{-1}). The vertical axis is a product of the $\mathrm{U_1}$ couplings, $h_L^{33} h_L^{23} \equiv h_{b\tau} h_{c\nu}$, and the horizontal one is the LQ mass, M_{LQ}. The region favored by $R_{D^{(*)}}$ at the $1\,\sigma$ ($2\,\sigma$) level is also given in the green (yellow) color. Regarding the $U(2)$-$\mathrm{U_1}$ scenario, the relative phase is fixed as $\phi_R = 0.42\pi$.

In the figure, the results are shown for $R_{s/b} \to 0$ and $R_{s/b} = 1$ in the left and right panels, respectively. The former corresponds to the single C_{V_1} scenario, and hence, the NP sensitivity is exactly the same as that given in the previous section. On the other hand, since $h_L^{23} = h_{s\tau} = h_{c\nu}$ in the $\mathrm{U_1}$ LQ model as aforementioned in Sec. 3.2, the latter indicates how $h_{s\tau} \neq 0$ contribution to the signal production affects the NP sensitivity. For $R_{s/b} = 1$, it is found that the $\tau^\pm\nu$ search can be competitive to that of $\tau^\pm\nu + b$. We also show the sensitivities for larger $R_{s/b}$ as $= 2, 4$ and 4 in the single-$\mathrm{U_1}$ and $U(2)$-$\mathrm{U_1}$ scenarios, respectively, at $M_{\mathrm{LQ}} = 4$ TeV for further comparison. It is concluded from the figures that both scenarios can be tested at HL-LHC with $\int \mathcal{L}\,dt = 3000$ fb^{-1}. Regarding the $U(2)$-$\mathrm{U_1}$ scenario, the present LHC data sample is large enough to probe the scenario if the $\tau^\pm\nu + b$ analysis is performed. Also, it should be mentioned that the result depends on $R_{s/b}$ significantly. It is shown that the sensitivities are enhanced by larger $R_{s/b}$ even in the EFT limit. Its contribution will be investigated in detail later.

Figure 5 shows a dependence of the LHC sensitivity on the LQ couplings, $h_L^{23} (= h_{s\tau} = h_{c\nu})$

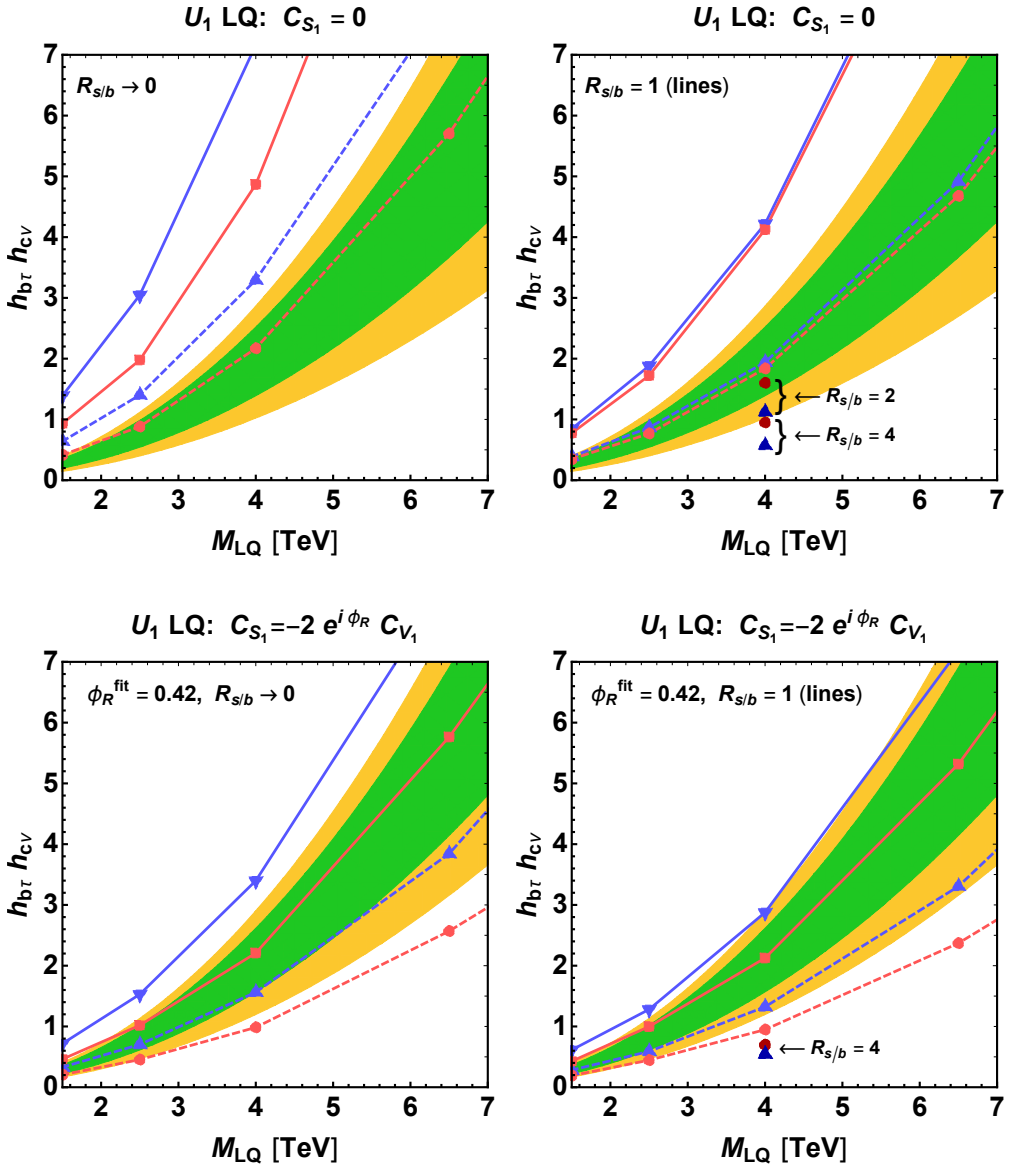

Figure 4. Expected sensitivities to the U_1 LQ scenario. The vertical axis is a product of the U_1 couplings, $h_L^{33}h_L^{23} \equiv h_{b\tau}h_{c\nu}$, and the horizontal one is the LQ mass, $M_{\rm LQ}$. Here, $R_{s/b} \to 0$ and $R_{s/b} = 1$ in the left and right panels, respectively. The $R_{D^{(*)}}$ anomaly is solved at the $1\,\sigma$ (green) and $2\,\sigma$ (yellow) levels. See Fig. 1 for the conventions of the plot markers and colors. The sensitivities for $R_{s/b} = 2, 4$ and 4 are also shown in the single-U_1 and $U(2)$-U_1 scenarios, respectively, at $M_{\rm LQ} = 4$ TeV.

and $h_L^{33}(= h_{b\tau})$ for $M_{\rm LQ} = 2$ and 4 TeV. One can see that, for both scenarios, the result in the $\tau^\pm\nu + b$ search is sensitive to large $h_{b\tau}$ and small $h_{s\tau}$, namely small $R_{s/b}$, whereas that of $\tau^\pm\nu$ is sensitive to larger $R_{s/b}$. For the single-U_1 scenario, the region favored by $R_{D^{(*)}}$ can be tested at $\int \mathcal{L}\,dt = 3000\,{\rm fb}^{-1}$ by the $\tau^\pm\nu(+b)$ search only for $h_{s\tau} \gtrsim 0.8(1.1)$ with $M_{\rm LQ} = 2$ TeV, and for $h_{s\tau} \gtrsim 1.5(2.0)$ with $M_{\rm LQ} = 4$ TeV. As for $U(2)$-U_1, on the other hand, the $R_{D^{(*)}}$-favored region is fully probed by $\tau^\pm\nu + b$ at $\int \mathcal{L}\,dt = 3000\,{\rm fb}^{-1}$ for both $M_{\rm LQ} = 2, 4$ TeV.

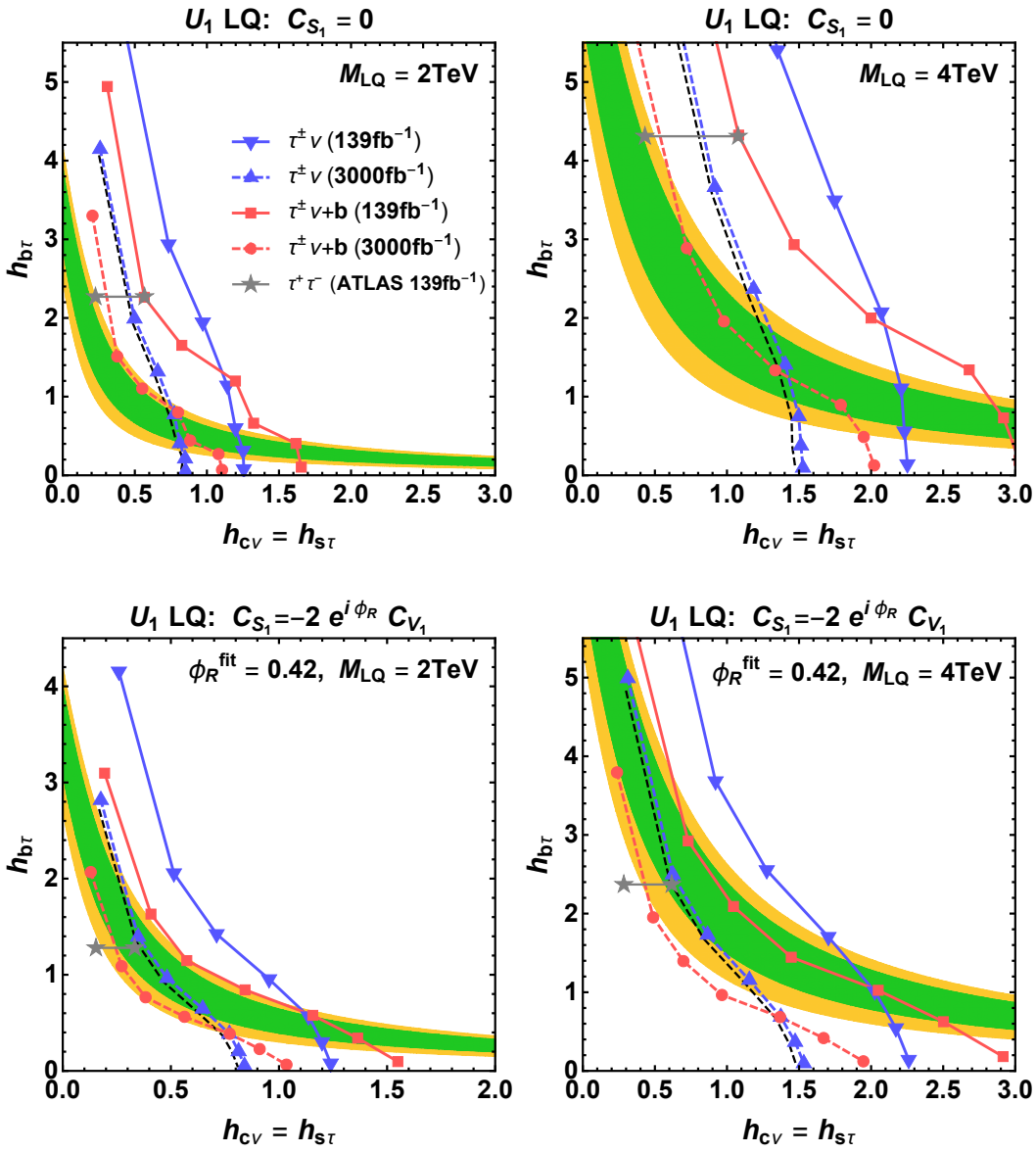

Figure 5. Expected sensitivities to the U_1 LQ scenario as functions of the LQ couplings with the LQ mass of 2 TeV (left) and 4 TeV (right). The black dashed lines show the results with selecting $\tau^-\nu$. The gray horizontal lines correspond to the current LHC bound recast from the ATLAS $pp \to \tau^+\tau^-$ search. See Fig. 4 for other color conventions.

In Ref. [72], the $pp \to \tau^+\tau^-$ search by the ATLAS [73] has been used to constrain the present two U_1 LQ scenarios.[#8] Their definition of the LQ couplings are related to ours as $h_{b\tau} \equiv g_U \beta_L^{b\tau}$ and $h_{s\tau} \equiv g_U \beta_L^{s\tau}$ by taking $\beta_L^{b\tau} = 1$. Then, the upper limit on $(g_U, M_{\rm LQ})$ has been recast from the ATLAS result at $\int \mathcal{L}\, dt = 139\,\text{fb}^{-1}$, where $\beta_L^{s\tau} \supset [0.10, 0.25]$ ($[0.12, 0.26]$) is fitted from relevant flavor observables for single-U_1 ($U(2)$-U_1). Although it is unclear how to implement the sub-

[#8] References [74, 75] also provide bounds on the LQ scenarios from the $pp \to \tau^+\tau^-$ search.

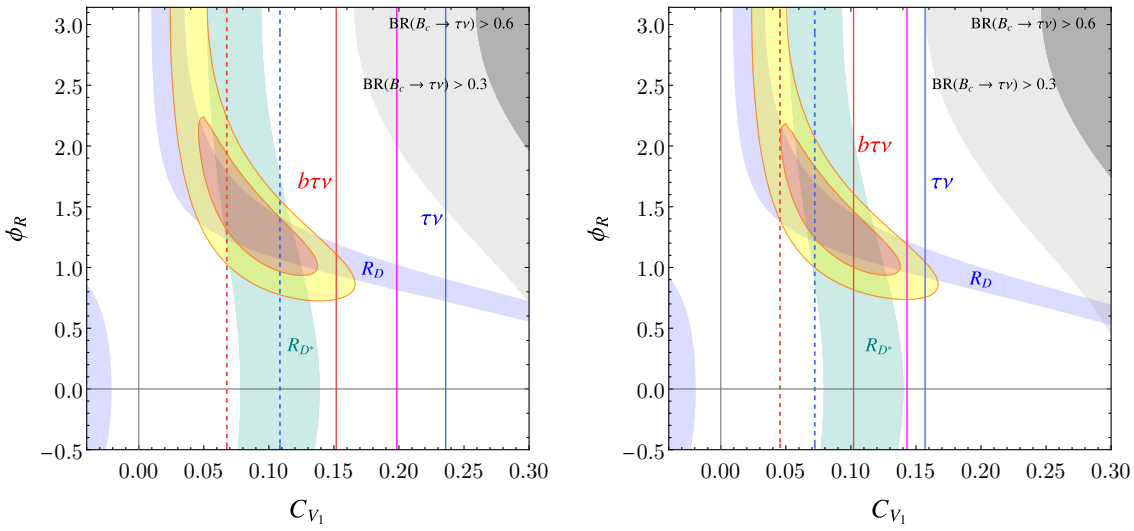

(a) $M_{\mathrm{U_1\,LQ}} = 1.5$ TeV (b) $M_{\mathrm{U_1\,LQ}} = 4.0$ TeV

Figure 6. The $U(2)$-$\mathrm{U_1}$ scenario with $M_{\mathrm{LQ}} = 1.5$ and 4.0 TeV on the (C_{V_1}, ϕ_R) plane. The color convention is the same as in Fig. 2. The magenta lines correspond to the current bound from the experimental data with $\int \mathcal{L}\,dt = 36\,\mathrm{fb}^{-1}$ by assuming $M_{\mathrm{LQ}} = 2$ TeV (left panel) and the EFT limit (right panel) [35].

leading contributions from $bs/ss \to \tau^+\tau^-$ in their study, we naively translate their result into the $(h_{s\tau}, h_{b\tau})$ plane as shown in the figure with gray lines. It is found that the $\tau^\pm\nu + b$ search is complementary to that of $\tau^+\tau^-$, though further discussions are needed on the analysis.

In Fig. 6, the $R_{D^{(*)}}$-favored region is compared with the LHC sensitivities and flavor constraints for $M_{\mathrm{LQ}} = 1.5$ TeV (left) and 4 TeV (right) in the $U(2)$-$\mathrm{U_1}$ scenario on the (C_{V_1}, ϕ_R) plane. The region in the right-hand side of the vertical (solid/dashed) lines is probed or constrained by the LHC searches. The orange (yellow) region is favored by the measured $R_{D^{(*)}}$ at the $1\,\sigma$ ($2\,\sigma$) level. Note that the best fit is given at $\phi_R \simeq \pm 0.42\pi$, implying $C_{S_1}/C_{V_1} \simeq -0.50 \mp 1.94i$. Similar to the $\mathrm{R_2}$ LQ model, imaginary component is favored to be large.[#9] From this figure, we found that the $R_{D^{(*)}}$-favored region can be fully (mostly) probed by $\tau^\pm\nu + b$ at $\int \mathcal{L}\,dt = 3000\,\mathrm{fb}^{-1}$ for $M_{\mathrm{LQ}} > 4$ TeV (< 4 TeV).

Similar to the $\mathrm{S_1}$ LQ scenario, there is a strong bound from ΔM_s, as briefly mentioned in Sec. 2.1. In realistic model setups of the $\mathrm{U_1}$ LQ scenario, vector-like leptons are introduced to realize a model flavor structure appropriately [43, 44, 76–78]. Their mass scale is comparable to the LQ one up to a factor depending on gauge and Yukawa couplings. Then, the GIM-like mechanism does work and the box contributions to ΔM_s are suppressed. Since the vector-like lepton mass determines an energy scale of the breakdown of the GIM-like cancellation, it cannot become too large, *i.e.*, must be around the TeV scale at most.[#10] To summarize, model predictions

[#9] Phase degrees of freedom are not taken into account in the parameter fit in literature [72, 76].

[#10] In such a case, three-body decay branching ratios (mediated by $\mathrm{U_1}$ LQ) of the vector-like leptons become dominant, and conventional searches [79, 80] are not applicable directly. The dedicated search for such a vector-like lepton at the LHC would be, therefore, important to probe a footprint of the LQ scenarios behind the B anomalies.

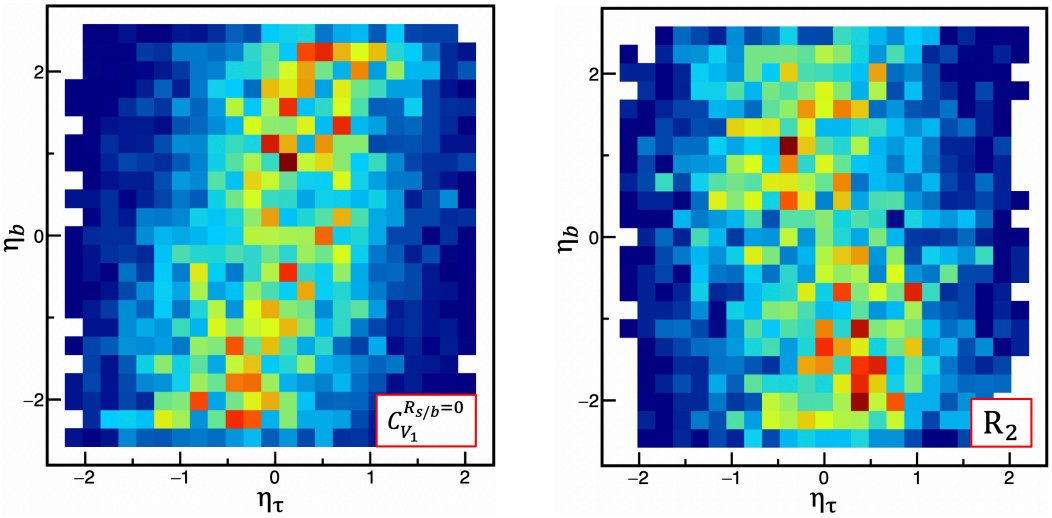

Figure 7. Distribution of signal number density in η_τ–η_b plane for the single-U$_1$ ($C_{V_1}^{R_{s/b}=0}$) (left) and single-R$_2$ (C_{S_2}) (right). In both scenarios, the LQ mass is set to be 1.5 TeV. The warmer/reddish (colder/bluish) colors represent larger (smaller) number of signal events.

of ΔM_s are quite model-dependent in the U$_1$ LQ scenarios, and dedicated studies are necessary. In Figs. 4 and 5, we do not draw the bounds from ΔM_s, for simplicity.

4.5 Angular correlations

We investigate the angular distributions in the $\tau^\pm\nu + b$ searches, which would be helpful to distinguish new physics scenarios and to further suppress the background. Requiring an additional b-jet not only amplifies sensitivity of new physics search, but also provides us information of the angular observables. Since the LQ models are characterized by the Lorentz structure of new physics interactions and the angular distributions of the final state are sensitive to them according to the analytic formulae of the scattering cross sections in Ref. [34], they are useful to discriminate the models.

Let us first demonstrate a correlation between the pseudorapidities of the bottom quark (η_b) and of the τ lepton (η_τ). Figure 7 shows a pseudorapidity correlation in the single-U$_1$(C_{V_1}) scenario with $R_{s/b} = 0$ (left) and the single-R$_2$(C_{S_2}) scenario (right) for $M_{\rm LQ} = 1.5$ TeV. Here, the LQ signal events passing **cut b** with $m_{\rm T} \geq 700$ GeV are exhibited. There are larger (smaller) number of signal events left after the cut in the reddish (blueish) points. As observed in the single-U$_1$(C_{V_1}) scenario (left panel), their positive correlation indicates that b and τ jets tend to be emitted in the same direction in the detector. On the other hand, the single-R$_2$(C_{S_2}) scenario (right panel) predicts a mild opposite correlation. Since the signal distribution on the (η_τ, η_b) plane depends on the NP scenarios, they could be distinguished by measuring the pseudorapidity correlation. It is noted that the same tendency is observed for $M_{\rm LQ} = 20$ TeV. Moreover, it is found that distributions in a case of $R_{s/b} = 1$ are similar to those for $R_{s/b} = 0$. This is because a contribution from the $\bar{s}$–τ–U$_1$ interaction, which comes from the b-jet mis-tagged from c-jet, is negligible in the $\tau^\pm\nu + b$ events for $R_{s/b} \lesssim 1$ (see Fig. 4).

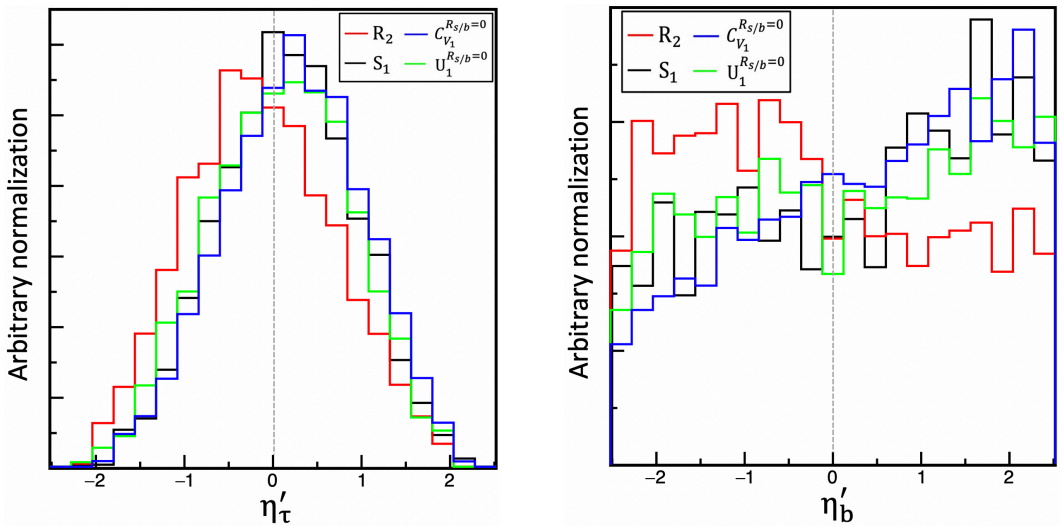

Figure 8. Distribution of signal event numbers against the modified pseudorapidity η'_τ (left) and η'_b (right) defined by Eq. (19) in the scenarios of single-R$_2$(C_{S_2}) (red), S$_1$ (black), single-U$_1$ ($C_{V_1}^{R_{s/b}=0}$) (blue), and $U(2)$-U$_1^{R_{s/b}=0}$ (light green). Here, $M_{\rm LQ} = 1.5$ TeV is taken, and the normalization of each histogram is arbitrary.

With having these observations, we propose the following quantities to probe the pseudorapidity correlation:

$$\eta'_\tau = {\rm sgn}(\eta_b) \times \eta_\tau\,, \qquad \eta'_b = {\rm sgn}(\eta_\tau) \times \eta_b\,. \tag{19}$$

For instance, the former is a modification of η_τ according to the b-jet direction. If a distribution of the b-jet is isotropic, a peak of η'_τ distribution must be placed at zero. However, events in the quadrants I and III of Fig. 7 provide a positive η'_τ, while the others yield a negative η'_τ. As a result, when there is the positive (negative) pseudorapidity correlation, a peak of η'_τ distribution shifts in a positive (negative) direction. Figure 8 shows the signal event distribution against η'_τ (left) and η'_b (right) in the scenarios of single-R$_2$(C_{S_2}) (red), S$_1$ with $C_{V_1} = 0$ (black), single-U$_1$ (C_{V_1}) (blue), and $U(2)$-U$_1$ (light green). The event normalization for each histogram is taken to be arbitrary. As expected from Fig. 7, it is found that the single-R$_2$(C_{S_2}) and single-U$_1$ (C_{V_1}) scenarios have a peak in a negative and positive η'_τ (and also η'_b) region, respectively. In fact, the condition $m_{\rm T} \geq 700$ GeV leads to large amount of events around $\eta_\tau = 0$, while η_b tends to be isotropic. As a result, it is found that modification of the shape is clearer in the η'_b plane than η'_τ. It is also observed that for the S$_1$ and $U(2)$-U$_1$ scenarios predict larger numbers of signal events in the $\eta'_{\tau(b)} > 0$ region compared to $\eta'_{\tau(b)} < 0$.

The azimuthal angle could also provide a tool to discriminate the UV models. We study the relative azimuthal angles among τ, ν (missing transverse momentum) and b to distinguish the NP scenarios. We show $\Delta\phi(\vec{p}_{\rm T}^{\,\tau}, \vec{p}_{\rm T}^{\,b})$ (left) and $\Delta\phi(\vec{p}_{\rm T}^{\,\rm miss}, \vec{p}_{\rm T}^{\,b})$ (right) in Fig. 9. Note that $\Delta\phi(\vec{p}_{\rm T}^{\,\tau}, \vec{p}_{\rm T}^{\,\rm miss})$ distribution is already used in the cut as the back-to-back configuration: $\Delta\phi(\vec{p}_{\rm T}^{\,\tau}, \vec{p}_{\rm T}^{\,\rm miss}) \geq 2.4$. The color convention is the same as the Fig. 8. It is observed that the single-R$_2$(C_{S_2}) scenario has more events in $0 \leq \Delta\phi(\vec{p}_{\rm T}^{\,\tau}, \vec{p}_{\rm T}^{\,b}) \leq \pi/2$ than the rest of that region, while the S$_1$ scenario has more in

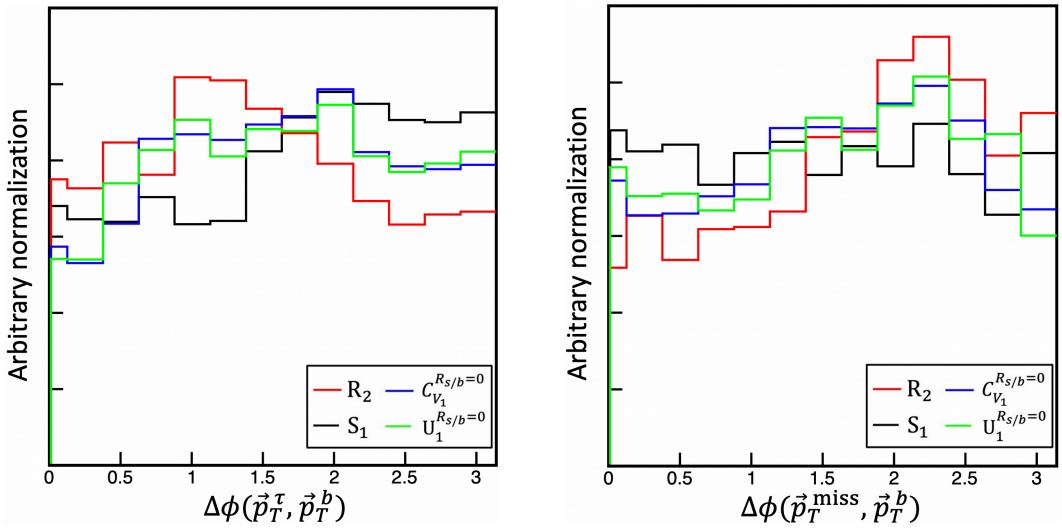

Figure 9. Distribution of signal event numbers against $\Delta\phi(\vec{p}_{\rm T}^{\,\tau}, \vec{p}_{\rm T}^{\,b})$ (left) and $\Delta\phi(\vec{p}_{\rm T}^{\,\rm miss}, \vec{p}_{\rm T}^{\,b})$ (right) in each LQ scenario. The color convention is the same as in Fig. 8. Here, $M_{\rm LQ} = 1.5$ TeV is taken, and the normalization of each histogram is arbitrary.

$\pi/2 \leq \Delta\phi(\vec{p}_{\rm T}^{\,\tau}, \vec{p}_{\rm T}^{\,b}) \leq \pi$. As for $\Delta\phi(\vec{p}_{\rm T}^{\,\rm miss}, \vec{p}_{\rm T}^{\,b})$, it is found that the single-$\mathrm{R}_2(C_{S_2})$ scenario has more events in $\pi/2 \leq \Delta\phi(\vec{p}_{\rm T}^{\,\rm miss}, \vec{p}_{\rm T}^{\,b}) \leq \pi$.

In conclusion, once signal events are measured, they would be helpful to discriminate the LQ models.

5 Conclusions and discussion

The $R_{D^{(*)}}$ anomaly is one of the hottest topics in the flavor physics from early in the last decade. Since the relevant $b \to c\tau\overline{\nu}$ process is induced by exchanging the W boson at the tree level within the SM and the observed deviation is $+\mathcal{O}(10)\%$ at the amplitude level, the NP scale is indicated at around 1–10 TeV to solve the $R_{D^{(*)}}$ anomaly. Among the NP models, the LQ particles have attracted a lot of interests. Such particles have been searched for by studying direct pair-production channels at the ATLAS and CMS, and the LQ mass has been constrained to be $> 1 - 1.5$ TeV. Although the next run will start at the LHC, if the mass is larger than $\gtrsim 2$ TeV, it is unlikely to discover the LQ directly in the near future. Nonetheless, thanks to the crossing symmetry of scattering amplitudes, the NP contributions to $b \to c\tau\overline{\nu}$ processes lead to $b\overline{c} \to \tau\overline{\nu}$ scattering at the LHC. Such a process was studied to probe the NP contributions indirectly even if the LQ is heavier than the LHC collision energy.

To amplify experimental sensitivities of such a non-resonant search, we examined the impact of requiring an additional b-jet in the final state, *e.g.*, $g\overline{c} \to \overline{b}\tau\overline{\nu}$. We evaluated the current and future LHC sensitivities based on both the EFT framework and the viable models of scalar- and vector-LQs; S_1, R_2, and U_1 with/without the $U(2)$ flavor symmetry. It was observed that the additional b-jet requirement and τ^- selection can improve the LHC sensitivity on the NP searches by $\approx 40\%$ and $\approx 10\%$ versus those in the $\tau^{\pm}\nu$ search, respectively. Furthermore, the LQ mass dependence

of the sensitivities is explicitly shown in the LQ mass range of $M_{\rm LQ} = \mathcal{O}(1)$ TeV for the $\tau^\pm\nu + b$ search as well as the $\tau^\pm\nu$ case. In particular, it was found that the sensitivity from the $\tau^\pm\nu + b$ search is better than that from $\tau^\pm\nu$ in the whole mass region for $R_{s/b} \lesssim 1$.

Based on those findings, the LHC sensitivities are compared with the parameter regions that can accommodate the $R_{D^{(*)}}$ anomaly in several single LQ scenarios. There are three types of viable leptoquark models responsible for the anomaly; the R_2, S_1, and U_1 LQ scenarios. We observed the following results:

- For the single-$R_2(C_{S_2})$ LQ scenario, it is found that the current LHC data of $\int \mathcal{L}\,dt = 139$ fb^{-1} are enough to probe the R_2 LQ, although the LQ mass dependence is crucial to claim whether the LQ is fully detectable. For instance, the $\tau^\pm\nu + b$ search with $\int \mathcal{L}\,dt = 139$ fb^{-1} fully covers the single-$R_2(C_{S_2})$ scenario with $M_{\rm LQ} > 2.5$ TeV responsible for the $R_{D^{(*)}}$ anomaly, while the region of 1.5 TeV $< M_{\rm LQ} <$ 2.5 TeV can be probed partially.

- For the S_1 LQ scenario, the parameter region is already severely constrained from $B \to K^*\nu\overline{\nu}$ and ΔM_s measurements, and the current LHC data can not test the allowed region. Larger luminosity such as the HL-LHC with requiring an additional b-jet is needed to probe these parameter regions.

- For the U_1 LQ scenarios, there are several parameter regions that can accommodate the $R_{D^{(*)}}$ anomaly depending on flavor structures of the LQ couplings and the LQ mass. It is found that the HL-LHC can probe the parameter regions in both the single-U_1 (C_{V_1}) and $U(2)$-U_1 scenarios by requiring an additional b-jet.

- As mentioned in Sec. 4.1, the ATLAS collaboration observed smaller number of events than the expected one in the $\tau^\pm\nu$ category at the data of $\int \mathcal{L}\,dt = 139$ fb^{-1}, and provided stronger constraint than the expectation [26]. Therefore, an experimental analysis with requiring an additional b-jet is of great importance. Particularly, the single-R_2 LQ scenario could be probed immediately by using the data of $\int \mathcal{L}\,dt = 139$ fb^{-1}.

The angular correlations among τ-, b-jets and missing transverse momentum were also studied. It was shown that the correlation between τ- and b-jets in the pseudorapidity plane could be useful to discriminate the LQ scenarios. Besides, it was found that the azimuthal angle distributions would also be helpful.

In this paper, models with light right-handed (sterile) neutrinos are not discussed. In those scenarios, WCs are likely to be large to explain the $R_{D^{(*)}}$ anomaly, because there is no interference with the SM amplitude. For instance, the effective Hamiltonian analogous to that of C_{V_1} is given as

$$\mathcal{H}_{\rm eff} = 2\sqrt{2} G_F V_{cb} C'_{V_1} (\overline{c}\gamma^\mu P_L b)(\overline{\tau}\gamma_\mu P_R \nu_\tau) + \text{h.c.}, \tag{20}$$

and $C'_{V_1} \approx 0.4 \pm 0.05$ can explain the $R_{D^{(*)}}$ anomaly. Since the LHC searches are expected to be insensitive to the neutrino chirality, we can apply the bound/sensitivity obtained for C_{V_1} to the right-handed neutrino scenario. It was shown that the current data of $\int \mathcal{L}\,dt = 139$ fb^{-1} are enough to probe $C'_{V_1} \gtrsim 0.2$ (0.3) in the EFT limit (for $M_{\rm LQ} = 1.5$ TeV) in the $\tau^\pm\nu_R + b$ search, see Table 6. Thus, the parameter region of C'_{V_1} favored by the $R_{D^{(*)}}$ anomaly can be tested immediately. Further improvements could be possible if larger amount of data is accumulated. In this work, we studied

events in the region of $m_{\rm T} > 1$ TeV to derive the NP sensitivities. With larger data, one could push the $m_{\rm T}$ condition to a larger side, *e.g.*, $m_{\rm T} > 2$ TeV. Then, the sensitivity would be improved by further suppression of the SM backgrounds. Moreover, further suppression of $\varepsilon_{j\to b}$ is expected to improve the sensitivity, since a large amount of the SM background events coming from fake b-jets can be reduced.

In the aspect of the flavor physics, q^2 distribution, D^* polarization and τ polarization in $\overline{B} \to D^{(*)}\tau\overline{\nu}$ as well as the other $b \to c\tau\overline{\nu}$ processes, *e.g.*, $B_c \to J/\psi\tau\overline{\nu}$, $\Lambda_b \to \Lambda_c\tau\overline{\nu}$, and $B_s \to D_s\tau\overline{\nu}$ will be important to cross check the NP scenarios in the next decade. It would be exciting to see how the data evolves once we are moving to the higher precision. Since the LHC and Belle II experiments enjoy the high statistic era in this and next decades, the interplay between the flavor physics and collider physics would become more significant.

Acknowledgement

We thank Tomomi Kawaguchi and Yuta Takahashi for valuable comments and discussion on the flavor tagging at the LHC. We also thank Sho Iwamoto for useful comments on MADGRAPH5_aMC@NLO. We appreciate Kazuhiro Tobe and Yuki Otsu for fruitful discussion on the relation between $\Delta F = 2$ observables and LQs. This work is supported by the Grant-in-Aid for Scientific Research on Innovative Areas (No. 21H00086 [ME] and No. 19H04613 [MT]), Scientific Research B (No. 21H01086 [ME]), Scientific Research C (No. 18K03611 [MT]), Early-Career Scientists (No. 16K17681 [ME] and No. 19K14706 [TK]), and JSPS Fellows (No. 19J10980 [SI]) from the Ministry of Education, Culture, Sports, Science, and Technology (MEXT), Japan. The work of S. I. is supported by the World Premier International Research Center Initiative (WPI), MEXT, Japan (Kavli IPMU). The work of S. I., T. K., and M. T. is also supported by the JSPS Core-to-Core Program (Grant No. JPJSCCA20200002). R. W. is partially supported by the INFN grant 'FLAVOR' and the PRIN 2017L5W2PT. S. I thanks the Yukawa Institute for Theoretical Physics at Kyoto University, where this work was initiated during the YITP-W-19-05 on "Progress in Particle Physics 2019". S. I appreciates Yuji Omura and C. -P. Yuan for the stimulating discussion at the initial stage.

A Simulation details

Here, we present some details of our MC setup and the signal and background cut flows, whose final results are summarized in in Sec. 4.1.

Event generations and hadronizations are done as described in Sec. 3 with the following details; as for a jet matching scale, `qCut = 45 GeV` is used to obtain the merged cross section; regarding the SM background, a model of "`sm-no_b_mass`" in MADGRAPH5 is used, which sets the bottom quark mass to be 0 while keeping the Yukawa coupling non-vanishing. For the NP signal, the bottom mass is set to be 0.

In the MC simulation, the following pre-cuts are imposed at the `run_card` level to reduce the computation cost:

$$p_{\rm T}^{\tau} \geq 200\,{\rm GeV}\,, \quad E_{\rm T}^{\rm miss} \geq 200\,{\rm GeV}\,, \quad |\eta_\tau| \leq 5\,, \quad \texttt{maxjetflavor} = 5\,, \tag{21}$$

BG (**cut a**)	Wjj	Zjj ($Z \to \nu\bar{\nu}$)	$t\bar{t}$	Z,γ DY	VV	single t
τ cut (a-1)	4613.3	562.0	241.8	1236.4	72.2	52.4
lepton cut (a-2)	4609.1	561.9	230.3	744.1	65.5	50.1
MET cut (a-3)	2933.0	471.9	190.8	83.9	42.8	42.6
back-to-back (a-4)	777.0	184.6	9.85	52.5	12.1	1.09
$0.7 < m_{\rm T} < 1$ TeV	70.5	20.1	0.34	3.03	1.30	0.02
1 TeV $< m_{\rm T}$	16.9	5.1	0.06	0.56	0.32	0.02
1 TeV $< m_{\rm T}$ [25]	22 ± 6.2	0.9 ± 0.5	< 0.1	< 0.1	0.7 ± 0.1	< 0.1
1 TeV $< m_{\rm T}$ [34]	18	5.2	0.44	0.0025	1.7	0.1

Table 9. Cut flows of the SM background events in the **cut a** category (the $\tau^{\pm}\nu$ search). The expected number of events corresponding to $\int \mathcal{L}\,dt = 35.9$ fb^{-1} at $\sqrt{s} = 13$ TeV are shown. The last two rows show the results by Refs. [25] and [34]. See, the main text for the detail.

and `JetMatching:nJetMax=-1` (default number) is set. The number of generated background events are 5M for Wjj, 40M for Zjj, 5M for $t\bar{t}$ with both W bosons decaying to τ, 5M for $t\bar{t}$ with one of the W bosons decaying to τ, 5M for $t+j$, 6M for $tW(1)$, 1M for $tW(2)$, 0.5M for $tZ(1)$, 5M for Z,γ DY, and 3M for each WW, $ZZ(\gamma)$, and $WZ(\gamma)$ categories. For the signal simulations, 100K events are generated in each model point of the NP signals. We have checked that the $m_{\rm T}$ distributions after the **cut a** and **cut b** are well smooth for each SM background category and the LQ signal. For the analysis of angular distributions discussed in Sec. 4.5, we increased the generated event numbers by factors to suppress the MC-statistical uncertainty appropriately.

Tables 9 and 10 are detailed cut flows of the SM background for the **cut a** and **cut b**, respectively. As a comparison with literature, we show the results of Refs. [25] and [34] for **cut a** and Ref. [34] for **cut b**. It should be noted that some details in the analysis procedures are different from ours; particularly, the b-tagging efficiencies (different from Ref. [34] for **cut b**), the jet cone size (different from Ref. [25] for **cut a** and **cut b**), hadronic τ tagging method (not explained in Ref. [34] explicitly, and different from Ref. [25], for **cut a** and **cut b**), and so on. As for **cut a** the differences are expected to hardly affect the results, and we found that our result is consistent with those in Refs. [25] and [34].

On the other hand, out result for **cut b** is well suppressed versus those in Ref. [34]. This is mainly because we used a working point with smaller b mis-tagging rates.

Tables 11, 12, 13, and 14 are detailed cut flows of the LQ signal for **cut a** and **cut b**. See the caption of Table 3 for the details.

B Flavor observables

In this appendix, the S_1 LQ contributions to $B \to K^{(*)}\nu\bar{\nu}$ and B_s–$\bar{B}_s$ mixing are discussed.

BG (**cut b**)	Wjj	$Zjj\,(Z\to\nu\bar{\nu})$	$t\bar{t}$	Z,γ DY	VV	single t
number of jets	6693.4	235099	346.7	1813.2	125.8	151.8
number of τ	3173.5	5617.1	73.9	894.9	59.7	34.0
number of b	90.6	305.5	35.9	163.9	5.28	18.8
isolated lepton	90.5	305.5	29.7	10.4	1.38	17.0
τ kinematics	78.8	20.8	23.6	9.19	1.13	14.0
MET cut	71.2	4.62	20.9	2.52	0.98	12.7
back-to-back	7.84	3.61	1.67	0.57	0.18	0.54
$0.7 < m_{\rm T} < 1$ TeV	0.58	0.37	0.056	0.28	0.018	0.029
1 TeV $< m_{\rm T}$	0.16	0.06	0.01	0.007	0.005	0.005
1 TeV $< m_{\rm T}$ [34]	0.18(5)	0.21(12)	0.29(3)	$4.2(4)\times10^{-5}$	0.35(5)	0.067(7)

Table 10. Same as Table 9 but for **cut b** (the $\tau^{\pm}\nu+b$ search). The last row shows the results by Ref. [34]. Note that their b-tagging efficiencies are different from ours (see, the footnote #3).

	$C_{V_1,1.5\text{ TeV}}$	$C_{V_1,\text{EFT}}$	$C^{R_{s/b}=1}_{V_1,1.5\text{ TeV}}$	$C^{R_{s/b}=1}_{V_1,\text{EFT}}$	BG
τ cut (a-1)	889	1198	2182	2876	6778
lepton cut (a-2)	888	1198	2180	2874	6261
MET cut (a-3)	539	783	1319	1861	3765
back-to-back (a-4)	452	577	1015	1483	1030
$0.7 < m_{\rm T} < 1$ TeV	90.0	139.4	225.9	351.4	95.3
1 TeV $< m_{\rm T}$	54.4	123.6	146.9	345.8	23.0

Table 11. Cut flows of the signal event numbers in the **cut a** category for several setups of the C_{V_1} scenario with $C_{V_1}=1$ and $\int\mathcal{L}dt = 35.9\,\text{fb}^{-1}$. See the caption of Table 3 for the details.

A ratios between the measured branching fractions of $B\to K^{(*)}\nu\bar{\nu}$ and the SM predictions is represented by $\mathcal{R}^{\nu\bar{\nu}}_{K^{(*)}}$ [81]. For a case of the minimal coupling of the S_1 LQ scenario, we obtain [82]

$$\mathcal{R}^{\nu\bar{\nu}}_{K^{(*)}} = \frac{2}{3} + \frac{1}{3}\frac{\left|C^{\text{SM},33}_{L,sb} + C^{\text{NP},33}_{L,sb}\right|^2}{\left|C^{\text{SM},33}_{L,sb}\right|^2}, \tag{22}$$

with

$$C^{\text{NP},33}_{L,sb} \simeq +2\frac{\pi}{\alpha}C_{V_1}, \qquad C^{\text{SM},33}_{L,sb} \simeq -\frac{1.47}{\sin^2\theta_{\text{W}}}, \tag{23}$$

	$U_{1,1.5\,\mathrm{TeV}}^{R_{s/b}=0}$	$U_{1,\mathrm{EFT}}^{R_{s/b}=0}$	$U_{1,1.5\,\mathrm{TeV}}^{R_{s/b}=1}$	$U_{1,\mathrm{EFT}}^{R_{s/b}=1}$	BG
τ cut (a-1)	2875	4189	4106	6003	6778
lepton cut (a-2)	2871	4184	4103	5999	6261
MET cut (a-3)	1863	2934	2672	4123	3765
back-to-back (a-4)	1530	2423	2108	3409	1030
$0.7 < m_{\mathrm{T}} < 1$ TeV	361	582	502	809	95.3
1 TeV $< m_{\mathrm{T}}$	204	571	279	799	23.0

Table 12. Same as Table 11 but for the U_1 LQ scenario with the $U(2)$ flavor symmetry, where $C_{V_1} = 1$ and $\int \mathcal{L}\,dt = 35.9\,\mathrm{fb}^{-1}$.

	$C_{V_1,1.5\,\mathrm{TeV}}$	$C_{V_1,\mathrm{EFT}}$	$C_{V_1,1.5\,\mathrm{TeV}}^{R_{s/b}=1}$	$C_{V_1,\mathrm{EFT}}^{R_{s/b}=1}$	BG
number of jets	1529	1873	3290	4283	244230
number of τ	693	907	1576	2114	9853
number of b	144	182	178	237	620.0
isolated lepton	142	180	177	234	454.5
τ kinematics	128	165	156	210	147.5
MET cut	99.5	131	125	169	112.9
back-to-back	48.5	84.3	76.0	111	14.4
$0.7 < m_{\mathrm{T}} < 1$ TeV	11.6	16.6	13.9	21.7	1.33
1 TeV $< m_{\mathrm{T}}$	6.51	14.6	9.39	21.6	0.25

Table 13. Same as Table 11 but in the **cut b** category. See the caption of Table 4 for the details.

and

$$\mathcal{H}_{\mathrm{eff}}^{\nu\nu} = -\frac{G_F \alpha}{\sqrt{2}\pi} V_{tb} V_{ts}^* C_{L,sb}^{fi} \left(\bar{s}\gamma^\mu P_L b\right) \left(\bar{\nu}_f \gamma_\mu (1-\gamma_5)\nu_i\right) + \mathrm{h.c.}\,, \tag{24}$$

where there are no QCD corrections from the RG evolution. Note that the WC, C_{V_1}, is defined by the effective Hamiltonian in Eq. (1). The Belle collaboration has provided a severe upper bound on $B \to K^* \nu\bar{\nu}$ as $\mathcal{R}_{K^*}^{\nu\bar{\nu}} < 2.7$ at the 90% C.L. [83]. From these numbers, we obtain

$$-0.011 < C_{V_1} < 0.027\,, \tag{25}$$

	$U_{1,1.5\,\mathrm{TeV}}^{R_{s/b}=0}$	$U_{1,\mathrm{EFT}}^{R_{s/b}=0}$	$U_{1,1.5\,\mathrm{TeV}}^{R_{s/b}=1}$	$U_{1,\mathrm{EFT}}^{R_{s/b}=1}$	BG
number of jets	4245	6085	5966	8376	244230
number of τ	2024	2941	2898	4168	9853
number of b	460	692	535	754	620.0
isolated lepton	454	685	485	747	454.5
τ kinematics	424	637	451	692	147.5
MET cut	350	540	371	590	112.9
back-to-back	258	402	263	443	14.4
$0.7 < m_{\mathrm{T}} < 1$ TeV	53.9	86.4	55.8	92.0	1.33
1 TeV $< m_{\mathrm{T}}$	26.0	71.6	30.7	101	0.25

Table 14. Same as Table 13 but for the U_1 LQ scenario with the $U(2)$ flavor symmetry, where $C_{V_1} = 1$ and $\int \mathcal{L}\,dt = 35.9\,\mathrm{fb}^{-1}$.

for the S_1 LQ scenario. It is clearly seen that the S_1 LQ scenario is severely constrained (see Fig. 3). It is known, however, that adding $SU(2)_L$ triplet scalar LQ S_3 can alleviate the constraints from the $b \to s\nu\overline{\nu}$ processes due to a destructive interference [42, 70, 84].[#11]

Next, the S_1 LQ contribution to ΔM_s (via LQ–ν_τ box) is given as [70, 71]

$$\frac{\Delta M_s}{\Delta M_s^{\mathrm{SM}}} = \left| 1 + \frac{C_1^{\mathrm{NP}}}{C_1^{\mathrm{SM}}} \right| , \tag{26}$$

with

$$C_1^{\mathrm{NP}} \simeq \left(\frac{\alpha_s(M_{\mathrm{LQ}})}{\alpha_s(M_W)} \right)^{\frac{2}{7}} \frac{(V_{cb} G_F M_{\mathrm{LQ}})^2}{4\pi^2} C_{V_1}^2 , \qquad C_1^{\mathrm{SM}} = 2.35 \frac{(V_{tb} V_{ts}^* G_F M_W)^2}{4\pi^2} , \tag{27}$$

and

$$\mathcal{H}_{\mathrm{eff}} = C_1 \left(\bar{s}\gamma^\mu P_L b \right) \left(\bar{s}\gamma_\mu P_L b \right) . \tag{28}$$

Here, the WC, C_1, is given at the electroweak scale, and the prefactor $[\alpha_s(M_{\mathrm{LQ}})/\alpha_s(M_W)]^{\frac{2}{7}}$ is the leading QCD correction from the RG evolution [88]. Using the experimental data $\Delta M_s^{\mathrm{exp}} = (17.741 \pm 0.020)\,\mathrm{ps}^{-1}$ [21] and the SM prediction is $\Delta M_s^{\mathrm{SM}} = (18.4^{+0.7}_{-1.2})\,\mathrm{ps}^{-1}$ [89], one obtains the upper bound, $\Delta M_s/\Delta M_s^{\mathrm{SM}} < 1.11$, at $2\,\sigma$ level.

[#11] Such a singlet-triplet LQ model can also explain the $b \to s\ell^+\ell^-$ anomaly [85, 86] and the muon $g-2$ anomaly [87], simultaneously [70].

References

[1] **BaBar** Collaboration, "Evidence for an excess of $\bar{B} \to D^{(*)}\tau^-\bar{\nu}_\tau$ decays," Phys. Rev. Lett. **109** (2012) 101802 [arXiv:1205.5442].

[2] **BaBar** Collaboration, "Measurement of an Excess of $\bar{B} \to D^{(*)}\tau^-\bar{\nu}_\tau$ Decays and Implications for Charged Higgs Bosons," Phys. Rev. D **88** (2013) 072012 [arXiv:1303.0571].

[3] **Belle** Collaboration, "Measurement of the branching ratio of $\bar{B} \to D^{(*)}\tau^-\bar{\nu}_\tau$ relative to $\bar{B} \to D^{(*)}\ell^-\bar{\nu}_\ell$ decays with hadronic tagging at Belle," Phys. Rev. D **92** (2015) 072014 [arXiv:1507.03233].

[4] **Belle** Collaboration, "Measurement of the τ lepton polarization and $R(D^*)$ in the decay $\bar{B} \to D^*\tau^-\bar{\nu}_\tau$," Phys. Rev. Lett. **118** (2017) 211801 [arXiv:1612.00529].

[5] **Belle** Collaboration, "Measurement of the τ lepton polarization and $R(D^*)$ in the decay $\bar{B} \to D^*\tau^-\bar{\nu}_\tau$ with one-prong hadronic τ decays at Belle," Phys. Rev. D **97** (2018) 012004 [arXiv:1709.00129].

[6] **Belle** Collaboration, "Measurement of $\mathcal{R}(D)$ and $\mathcal{R}(D^*)$ with a semileptonic tagging method." arXiv:1904.08794.

[7] **Belle** Collaboration, "Measurement of $\mathcal{R}(D)$ and $\mathcal{R}(D^*)$ with a semileptonic tagging method," Phys. Rev. Lett. **124** (2020) 161803 [arXiv:1910.05864].

[8] **LHCb** Collaboration, "Measurement of the ratio of branching fractions $\mathcal{B}(\bar{B}^0 \to D^{*+}\tau^-\bar{\nu}_\tau)/\mathcal{B}(\bar{B}^0 \to D^{*+}\mu^-\bar{\nu}_\mu)$," Phys. Rev. Lett. **115** (2015) 111803 [arXiv:1506.08614]. [Erratum: Phys.Rev.Lett. 115, 159901 (2015)].

[9] **LHCb** Collaboration, "Measurement of the ratio of the $B^0 \to D^{*-}\tau^+\nu_\tau$ and $B^0 \to D^{*-}\mu^+\nu_\mu$ branching fractions using three-prong τ-lepton decays," Phys. Rev. Lett. **120** (2018) 171802 [arXiv:1708.08856].

[10] **LHCb** Collaboration, "Test of Lepton Flavor Universality by the measurement of the $B^0 \to D^{*-}\tau^+\nu_\tau$ branching fraction using three-prong τ decays," Phys. Rev. D **97** (2018) 072013 [arXiv:1711.02505].

[11] S. Iguro and R. Watanabe, "Bayesian fit analysis to full distribution data of $\overline{\mathrm{B}} \to \mathrm{D}^{(*)}\ell\overline{\nu}$: $|\mathrm{V_{cb}}|$ determination and new physics constraints," JHEP **08** (2020) 006 [arXiv:2004.10208].

[12] D. London and J. Matias, "B Flavour Anomalies: 2021 Theoretical Status Report." arXiv:2110.13270.

[13] M. Blanke, *et al.*, "Impact of polarization observables and $B_c \to \tau\nu$ on new physics explanations of the $b \to c\tau\nu$ anomaly," Phys. Rev. D **99** (2019) 075006 [arXiv:1811.09603].

[14] S. Iguro and Y. Omura, "Status of the semileptonic B decays and muon g-2 in general 2HDMs with right-handed neutrinos," JHEP **05** (2018) 173 [arXiv:1802.01732].

[15] P. Asadi, M. R. Buckley, and D. Shih, "It's all right(-handed neutrinos): a new W′ model for the $R_{D^{(*)}}$ anomaly," JHEP **09** (2018) 010 [arXiv:1804.04135].

[16] A. Greljo, D. J. Robinson, B. Shakya, and J. Zupan, "R($\mathrm{D}^{(*)}$) from W′ and right-handed neutrinos," JHEP **09** (2018) 169 [arXiv:1804.04642].

[17] D. J. Robinson, B. Shakya, and J. Zupan, "Right-handed neutrinos and R($\mathrm{D}^{(*)}$)," JHEP **02** (2019) 119 [arXiv:1807.04753].

[18] K. S. Babu, B. Dutta, and R. N. Mohapatra, "A theory of R(D^*, D) anomaly with right-handed currents," JHEP **01** (2019) 168 [arXiv:1811.04496].

[19] N. Cabibbo, "Unitary Symmetry and Leptonic Decays," Phys. Rev. Lett. **10** (1963) 531–533.

[20] M. Kobayashi and T. Maskawa, "CP Violation in the Renormalizable Theory of Weak Interaction," Prog. Theor. Phys. **49** (1973) 652–657.

[21] **Particle Data Group** Collaboration, "Review of Particle Physics," PTEP **2020** (2020) 083C01.

[22] L. Di Luzio and M. Nardecchia, "What is the scale of new physics behind the B-flavour anomalies?" Eur. Phys. J. C **77** (2017) 536 [arXiv:1706.01868].

[23] **CMS** Collaboration, "Search for W' decaying to tau lepton and neutrino in proton-proton collisions at $\sqrt{s} = 8$ TeV," Phys. Lett. B **755** (2016) 196–216 [arXiv:1508.04308].

[24] **ATLAS** Collaboration, "Search for High-Mass Resonances Decaying to $\tau\nu$ in pp Collisions at $\sqrt{s}$=13 TeV with the ATLAS Detector," Phys. Rev. Lett. **120** (2018) 161802 [arXiv:1801.06992].

[25] **CMS** Collaboration, "Search for a W' boson decaying to a τ lepton and a neutrino in proton-proton collisions at $\sqrt{s} = 13$ TeV," Phys. Lett. B **792** (2019) 107–131 [arXiv:1807.11421].

[26] **ATLAS** Collaboration, "Search for high-mass resonances in final states with a tau lepton and missing transverse momentum with the ATLAS detector," ATLAS–CONF–2021–025, CERN, 2021.

[27] D. A. Faroughy, A. Greljo, and J. F. Kamenik, "Confronting lepton flavor universality violation in B decays with high-p_T tau lepton searches at LHC," Phys. Lett. B **764** (2017) 126–134 [arXiv:1609.07138].

[28] S. Iguro, Y. Omura, and M. Takeuchi, "Test of the $R(D^{(*)})$ anomaly at the LHC," Phys. Rev. D **99** (2019) 075013 [arXiv:1810.05843].

[29] T. Mandal, S. Mitra, and S. Raz, "$R_{D^{(*)}}$ motivated $\mathcal{S}_1$ leptoquark scenarios: Impact of interference on the exclusion limits from LHC data," Phys. Rev. D **99** (2019) 055028 [arXiv:1811.03561].

[30] A. Greljo, J. Martin Camalich, and J. D. Ruiz-Álvarez, "Mono-τ Signatures at the LHC Constrain Explanations of B-decay Anomalies," Phys. Rev. Lett. **122** (2019) 131803 [arXiv:1811.07920].

[31] W. Altmannshofer, P. S. Bhupal Dev, and A. Soni, "$R_{D^{(*)}}$ anomaly: A possible hint for natural supersymmetry with R-parity violation," Phys. Rev. D **96** (2017) 095010 [arXiv:1704.06659].

[32] S. Iguro and K. Tobe, "$R(D^{(*)})$ in a general two Higgs doublet model," Nucl. Phys. B **925** (2017) 560–606 [arXiv:1708.06176].

[33] M. Abdullah, J. Calle, B. Dutta, A. Flórez, and D. Restrepo, "Probing a simplified, W' model of $R(D^{(*)})$ anomalies using b-tags, τ leptons and missing energy," Phys. Rev. D **98** (2018) 055016 [arXiv:1805.01869].

[34] D. Marzocca, U. Min, and M. Son, "Bottom-Flavored Mono-Tau Tails at the LHC," JHEP **12** (2020) 035 [arXiv:2008.07541].

[35] S. Iguro, M. Takeuchi, and R. Watanabe, "Testing leptoquark/EFT in $\bar{B} \to D^{(*)} l \bar{\nu}$ at the LHC," Eur. Phys. J. C **81** (2021) 406 [arXiv:2011.02486].

[36] **CMS** Collaboration, "Measurement of the differential cross section and charge asymmetry for inclusive pp $\to$ W$^{\pm}$ + X production at $\sqrt{s} = 8$ TeV," Eur. Phys. J. C **76** (2016) 469 [arXiv:1603.01803].

[37] T.-J. Hou *et al.*, "New CTEQ global analysis of quantum chromodynamics with high-precision data from the LHC," Phys. Rev. D **103** (2021) 014013 [arXiv:1912.10053].

[38] M. Blanke, *et al.*, "Addendum to "Impact of polarization observables and $B_c \to \tau\nu$ on new physics explanations of the $b \to c\tau\nu$ anomaly"," Phys. Rev. D **100** (2019) 035035 [arXiv:1905.08253].

[39] S. Iguro, T. Kitahara, Y. Omura, R. Watanabe, and K. Yamamoto, "D* polarization vs. $R_{D^{(*)}}$ anomalies in the leptoquark models," JHEP **02** (2019) 194 [arXiv:1811.08899].

[40] D. Buttazzo, A. Greljo, G. Isidori, and D. Marzocca, "B-physics anomalies: a guide to combined explanations," JHEP **11** (2017) 044 [arXiv:1706.07808].

[41] A. Angelescu, D. Bečirević, D. A. Faroughy, and O. Sumensari, "Closing the window on single leptoquark solutions to the B-physics anomalies," JHEP **10** (2018) 183 [arXiv:1808.08179].

[42] A. Crivellin, D. Müller, and T. Ota, "Simultaneous explanation of $R(D^{(*)})$ and $b \to s\mu^+\mu^-$: the last scalar leptoquarks standing," JHEP **09** (2017) 040 [arXiv:1703.09226].

[43] L. Di Luzio, J. Fuentes-Martin, A. Greljo, M. Nardecchia, and S. Renner, "Maximal Flavour Violation: a Cabibbo mechanism for leptoquarks," JHEP **11** (2018) 081 [arXiv:1808.00942].

[44] J. Fuentes-Martín, G. Isidori, M. König, and N. Selimović, "Vector Leptoquarks Beyond Tree Level III: Vector-like Fermions and Flavor-Changing Transitions," Phys. Rev. D **102** (2020) 115015 [arXiv:2009.11296].

[45] R. Barbieri, G. R. Dvali, and L. J. Hall, "Predictions from a U(2) flavor symmetry in supersymmetric theories," Phys. Lett. B **377** (1996) 76–82 [hep-ph/9512388].

[46] R. Barbieri, L. J. Hall, and A. Romanino, "Consequences of a U(2) flavor symmetry," Phys. Lett. B **401** (1997) 47–53 [hep-ph/9702315].

[47] R. Barbieri, G. Isidori, J. Jones-Perez, P. Lodone, and D. M. Straub, "$U(2)$ and Minimal Flavour Violation in Supersymmetry," Eur. Phys. J. C **71** (2011) 1725 [arXiv:1105.2296].

[48] R. Barbieri, P. Campli, G. Isidori, F. Sala, and D. M. Straub, "B-decay CP-asymmetries in SUSY with a $U(2)^3$ flavour symmetry," Eur. Phys. J. C **71** (2011) 1812 [arXiv:1108.5125].

[49] R. Barbieri, D. Buttazzo, F. Sala, and D. M. Straub, "Flavour physics from an approximate $U(2)^3$ symmetry," JHEP **07** (2012) 181 [arXiv:1203.4218].

[50] G. Blankenburg, G. Isidori, and J. Jones-Perez, "Neutrino Masses and LFV from Minimal Breaking of $U(3)^5$ and $U(2)^5$ flavor Symmetries," Eur. Phys. J. C **72** (2012) 2126 [arXiv:1204.0688].

[51] R. Barbieri, G. Isidori, A. Pattori, and F. Senia, "Anomalies in B-decays and $U(2)$ flavour symmetry," Eur. Phys. J. C **76** (2016) 67 [arXiv:1512.01560].

[52] J. Fuentes-Martín, G. Isidori, J. Pagès, and K. Yamamoto, "With or without U(2)? Probing non-standard flavor and helicity structures in semileptonic B decays," Phys. Lett. B **800** (2020) 135080 [arXiv:1909.02519].

[53] P. Asadi, *New solutions to the charged current B-anomalies*. PhD thesis, Rutgers U., Piscataway (main), 2019.

[54] A. Alloul, N. D. Christensen, C. Degrande, C. Duhr, and B. Fuks, "FeynRules 2.0 - A complete toolbox for tree-level phenomenology," Comput. Phys. Commun. **185** (2014) 2250–2300 [arXiv:1310.1921].

[55] J. Alwall, *et al.*, "The automated computation of tree-level and next-to-leading order differential cross sections, and their matching to parton shower simulations," JHEP **07** (2014) 079 [arXiv:1405.0301].

[56] T. Sjöstrand, *et al.*, "An introduction to PYTHIA 8.2," Comput. Phys. Commun. **191** (2015) 159–177 [arXiv:1410.3012].

[57] J. Alwall *et al.*, "Comparative study of various algorithms for the merging of parton showers and matrix elements in hadronic collisions," Eur. Phys. J. C **53** (2008) 473–500 [arXiv:0706.2569].

[58] R. D. Ball *et al.*, "Parton distributions with LHC data," Nucl. Phys. B **867** (2013) 244–289 [arXiv:1207.1303].

[59] **DELPHES 3** Collaboration, "DELPHES 3, A modular framework for fast simulation of a generic collider experiment," JHEP **02** (2014) 057 [arXiv:1307.6346].

[60] M. Cacciari, G. P. Salam, and G. Soyez, "The anti-k_t jet clustering algorithm," JHEP **04** (2008) 063 [arXiv:0802.1189].

[61] **CMS** Collaboration, "Performance of reconstruction and identification of τ leptons decaying to hadrons and ν_τ in pp collisions at $\sqrt{s} = 13$ TeV," JINST **13** (2018) P10005 [arXiv:1809.02816].

[62] **ATLAS** Collaboration, "ATLAS b-jet identification performance and efficiency measurement with $t\bar{t}$ events in pp collisions at $\sqrt{s} = 13$ TeV," Eur. Phys. J. C **79** (2019) 970 [arXiv:1907.05120].

[63] J. Fuentes-Martin, A. Greljo, J. Martin Camalich, and J. D. Ruiz-Alvarez, "Charm physics confronts high-p_T lepton tails," JHEP **11** (2020) 080 [arXiv:2003.12421].

[64] **ATLAS** Collaboration, "Search for new phenomena in pp collisions in final states with tau leptons, b-jets, and missing transverse momentum with the ATLAS detector." arXiv:2108.07665.

[65] **CMS** Collaboration, "Search for singly and pair-produced leptoquarks coupling to third-generation fermions in proton-proton collisions at s=13 TeV," Phys. Lett. B **819** (2021) 136446 [arXiv:2012.04178].

[66] R. Alonso, E. E. Jenkins, A. V. Manohar, and M. Trott, "Renormalization Group Evolution of the Standard Model Dimension Six Operators III: Gauge Coupling Dependence and Phenomenology," JHEP **04** (2014) 159 [arXiv:1312.2014].

[67] M. González-Alonso, J. Martin Camalich, and K. Mimouni, "Renormalization-group evolution of new physics contributions to (semi)leptonic meson decays," Phys. Lett. B **772** (2017) 777–785 [arXiv:1706.00410].

[68] J. Aebischer and B. Grinstein, "Standard Model prediction of the B_c lifetime," JHEP **07** (2021) 130 [arXiv:2105.02988].

[69] J. Aebischer and B. Grinstein, "A novel determination of the B_c lifetime." arXiv:2108.10285.

[70] A. Crivellin, D. Müller, and F. Saturnino, "Flavor Phenomenology of the Leptoquark Singlet-Triplet Model," JHEP **06** (2020) 020 [arXiv:1912.04224].

[71] A. Crivellin, J. F. Eguren, and J. Virto, "Next-to-Leading-Order QCD Matching for $\Delta F = 2$ Processes in Scalar Leptoquark Models." arXiv:2109.13600.

[72] C. Cornella, D. A. Faroughy, J. Fuentes-Martin, G. Isidori, and M. Neubert, "Reading the footprints of the B-meson flavor anomalies," JHEP **08** (2021) 050 [arXiv:2103.16558].

[73] **ATLAS** Collaboration, "Search for heavy Higgs bosons decaying into two tau leptons with the ATLAS detector using pp collisions at $\sqrt{s} = 13$ TeV," Phys. Rev. Lett. **125** (2020) 051801 [arXiv:2002.12223].

[74] U. Aydemir, T. Mandal, and S. Mitra, "Addressing the $\mathbf{R}_{D^{(*)}}$ anomalies with an $\mathbf{S}_1$ leptoquark from $\mathbf{SO(10)}$ grand unification," Phys. Rev. D **101** (2020) 015011 [arXiv:1902.08108].

[75] A. Bhaskar, D. Das, T. Mandal, S. Mitra, and C. Neeraj, "Precise limits on the charge-2/3 U1 vector leptoquark," Phys. Rev. D **104** (2021) 035016 [arXiv:2101.12069].

[76] C. Cornella, J. Fuentes-Martin, and G. Isidori, "Revisiting the vector leptoquark explanation of the B-physics anomalies," JHEP **07** (2019) 168 [arXiv:1903.11517].

[77] L. Calibbi, A. Crivellin, and T. Li, "Model of vector leptoquarks in view of the B-physics anomalies," Phys. Rev. D **98** (2018) 115002 [arXiv:1709.00692].

[78] S. Iguro, J. Kawamura, S. Okawa, and Y. Omura, "TeV-scale vector leptoquark from Pati-Salam unification with vectorlike families," Phys. Rev. D **104** (2021) 075008 [arXiv:2103.11889].

[79] N. Kumar and S. P. Martin, "Vectorlike Leptons at the Large Hadron Collider," Phys. Rev. D **92** (2015) 115018 [arXiv:1510.03456].

[80] **CMS** Collaboration, "Search for vector-like leptons in multilepton final states in proton-proton collisions at $\sqrt{s} = 13$ TeV," Phys. Rev. D **100** (2019) 052003 [arXiv:1905.10853].

[81] A. J. Buras, J. Girrbach-Noe, C. Niehoff, and D. M. Straub, "$B \to K^{(*)}\nu\overline{\nu}$ decays in the Standard Model and beyond," JHEP **02** (2015) 184 [arXiv:1409.4557].

[82] A. Carvunis, A. Crivellin, D. Guadagnoli, and S. Gangal, "The Forward-Backward Asymmetry in $B \to D^*\ell\nu$: One more hint for Scalar Leptoquarks?" arXiv:2106.09610.

[83] **Belle** Collaboration, "Search for $B \to h\nu\bar{\nu}$ decays with semileptonic tagging at Belle," Phys. Rev. D **96** (2017) 091101 [arXiv:1702.03224]. [Addendum: Phys.Rev.D 97, 099902 (2018)].

[84] V. Gherardi, D. Marzocca, and E. Venturini, "Low-energy phenomenology of scalar leptoquarks at one-loop accuracy," JHEP **01** (2021) 138 [arXiv:2008.09548].

[85] **LHCb** Collaboration, "Test of lepton universality with $B^0 \to K^{*0}\ell^+\ell^-$ decays," JHEP **08** (2017) 055 [arXiv:1705.05802].

[86] **LHCb** Collaboration, "Test of lepton universality in beauty-quark decays." arXiv:2103.11769.

[87] **Muon g-2** Collaboration, "Measurement of the Positive Muon Anomalous Magnetic Moment to 0.46 ppm," Phys. Rev. Lett. **126** (2021) 141801 [arXiv:2104.03281].

[88] J. A. Bagger, K. T. Matchev, and R.-J. Zhang, "QCD corrections to flavor changing neutral currents in the supersymmetric standard model," Phys. Lett. B **412** (1997) 77–85 [hep-ph/9707225].

[89] L. Di Luzio, M. Kirk, A. Lenz, and T. Rauh, "ΔM_s theory precision confronts flavour anomalies," JHEP **12** (2019) 009 [arXiv:1909.11087].